



Mobility & Vehicle Mechanics

*International Journal for Vehicle Mechanics, Engines and
Transportation Systems*

ISSN 1450 - 5304

UDC 621 + 629(05)=802.0

Miroslav Petrovic Aleksandar Davinic Nadica Stojanovic Ivan Grujic	INFLUENCE OF HYDROGEN INJECTION AND IGNITION PARAMETERS ON THE COMBUSTION PROCESS IN THE IC ENGINE	1-14
Miroslav Demic	DEVELOPMENT OF A METHOD FOR DEFINING THE TORSIONAL STIFFNESS OF THE FRAME IN THE INITIAL PHASE OF DESIGNING A HEAVY MOTOR VEHICLE	15-29
Vasile Blaga Mihai Blaga	THE STUDY OF THE PROCESSES THAT TAKE PLACE IN GASOLINE INJECTION ENGINES	31-46
Djordje Ivkovic Dragan Adamovic Dušan Arsic Nada Ratkovic Andjela Mitrovic Ružica Nikolic	REVIEW OF THE ADVANCED HIGH- STRENGTH STEELS USED IN AUTOMOTIVE INDUSTRY	47-64
Slavica Màèužic Saveljic Danijela Miloradovic	SIMULATION OF PEDESTRIAN THROW DISTANCE IN THE SOFTWARE PACKAGE PC-CRASH - COMPARISON WITH EXPERIMENT AND THEORY	65-75



M V M

Mobility Vehicle Mechanics

Editor: Prof. dr Jovanka Lukić

MVM Editorial Board
University of Kragujevac
Faculty of Engineering
Sestre Janjić 6, 34000 Kragujevac, Serbia
Tel.: +381/34/335990; Fax: + 381/34/333192

Prof. Dr **Belingardi Giovanni**
Politecnico di Torino,
Torino, ITALY

Dr Ing. **Ćučuz Stojan**
Visteon corporation,
Novi Jicin,
CZECH REPUBLIC

Prof. Dr **Demić Miroslav**
University of Kragujevac
Faculty of Engineering
Kragujevac, SERBIA

Prof. Dr **Fiala Ernest**
Wien, OESTERREICH

Prof. Dr **Gillespie D. Thomas**
University of Michigan,
Ann Arbor, Michigan, USA

Prof. Dr **Glišović Jasna**
University of Kragujevac
Faculty of Engineering
Kragujevac, SERBIA

Prof. Dr **Knapezyk Josef**
Politechniki Krakowskiej,
Krakow, POLAND

Prof. Dr **Krstić Božidar**
University of Kragujevac
Faculty of Engineering
Kragujevac, SERBIA

Prof. Dr **Mariotti G. Virzi**
Universita degli Studidi Palermo,
Dipartimento di Meccanica ed
Aeronautica,
Palermo, ITALY

Prof. Dr **Miloradović Danijela**
University of Kragujevac
Faculty of Engineering
Kragujevac, SERBIA

Prof. Dr **Pešić Radivoje**
University of Kragujevac
Faculty of Engineering
Kragujevac, SERBIA

Prof. Dr **Petković Snežana**
University of Banja Luka
Faculty of Mech. Eng.
Banja Luka
REPUBLIC OF SRPSKA

Prof. Dr **Radonjić Rajko**
University of Kragujevac
Faculty of Engineering
Kragujevac, SERBIA

Prof. Dr **Spentzas Constantinos**
N. National Technical University,
GREECE

Prof. Dr **Todorović Jovan**
Faculty of Mech. Eng. Belgrade,
SERBIA

Prof. Dr **Toliskyj Vladimir E.**
Academician NAMI,
Moscow, RUSSIA

Prof. Dr **Teodorović Dušan**
Faculty of Traffic and Transport
Engineering,
Belgrade, SERBIA

Prof. Dr **Veinović Stevan**
University of Kragujevac
Faculty of Engineering
Kragujevac, SERBIA

For Publisher: Prof. dr Slobodan Savić, dean, University of Kragujevac, Faculty of Engineering

*Publishing of this Journal is financially supported from:
Ministry of Education, Science and Technological Development, Republic Serbia*

Mobility &

Motorna

Vehicle

Volume 49
Number 3
2023.

Vozila i

Mechanics

Motori

Miroslav Petrović
Aleksandar Davinić
Nadica Stojanović
Ivan Grujić

INFLUENCE OF HYDROGEN
INJECTION AND IGNITION
PARAMETERS ON THE COMBUSTION
PROCESS IN THE IC ENGINE

1-14

Miroslav Demić

DEVELOPMENT OF A METHOD FOR
DEFINING THE TORSIONAL
STIFFNESS OF THE FRAME IN THE
INITIAL PHASE OF DESIGNING A
HEAVY MOTOR VEHICLE

15-29

Vasile Blaga
Mihai Blaga

THE STUDY OF THE PROCESSES
THAT TAKE PLACE IN GASOLINE
INJECTION ENGINES

31-46

Djordje Ivković
Dragan Adamović
Dušan Arsić
Nada Ratković
Andjela Mitrović
Ružica Nikolić

REVIEW OF THE ADVANCED HIGH-
STRENGTH STEELS USED IN
AUTOMOTIVE INDUSTRY

47-64

Slavica Mačužić
Saveljić
Danijela Miloradović

SIMULATION OF PEDESTRIAN THROW
DISTANCE IN THE SOFTWARE
PACKAGE PC-CRASH - COMPARISON
WITH EXPERIMENT AND THEORY

65-75

Mobility &

Vehicle

Mechanics

Motorna

Vozila i

Motori

Volume 49
Number 3
2023.

Miroslav Petrović
Aleksandar Davinić
Nadica Stojanović
Ivan Grujić

UTICAJ PARAMETARA UBRIZGAVANJA
I PALJENJA VODONIKA NA PROCES
SAGOREVANJA U MOTORU SUS

1-14

Miroslav Demić

PRIOLOG RAZVOJU METODE ZA
DEFINISANJE TORZIONE KRUTOSTI
OKVIRA U FAZI IZRADE IDEJNOG
PROJEKTA TERETNOG MOTORNOG
VOZILA

15-29

Vasile Blaga
Mihai Blaga

PROUČAVANJE PROCESA KOJI SE
ODVIJAJU U MOTORIMA SA
UBRIZGAVANJEM BENZINA

31-46

Djordje Ivković
Dragan Adamović
Dušan Arsić
Nada Ratković
Andjela Mitrović
Ružica Nikolić

PREGLED NAPREDNIH ČELIKA
POVIŠENE JAČINE KORIŠĆENIH U
AUTOMOBILSKOJ INDUSTRIJI

47-64

Slavica Mačužić
Saveljić
Danijela Miloradović

SIMULACIJA DUŽINE ODBAČAJA
PEŠKA U PROGRAMSKOM PAKETU
PC-CRASH - POREĐENJE
EKSPERIMENTA I TEORIJE

65-75



INFLUENCE OF HYDROGEN INJECTION AND IGNITION PARAMETERS ON THE COMBUSTION PROCESS IN THE IC ENGINE

Miroslav Petrović^{1*}, Aleksandar Davinić², Nadica Stojanović³, Ivan Grujić⁴

Received in August 2023

Revised in September 2023


Accepted in October 2023


RESEARCH ARTICLE


ABSTRACT: Given that the trend of using vehicles has been increasing in recent decades, and as oil reserves are limited and environmental requirements are increasing, there is nothing left but to look for alternative solutions as a replacement for oil derivatives. Alternatives are electric vehicles and hybrid vehicles, but internal combustion engines (IC) should not be written off, alternative fuels such as liquefied petroleum gas (LPG) and compressed natural gas (CNG) are used for spark ignition (SI) engines. There is another alternative fuel for IC engines that is still being tested for use in vehicles, and that is hydrogen (H₂). There are still not many published results on hydrogen as a propellant. This paper will present the results of experimental research on the IC engine with hydrogen as a propellant, and the results refer to the parameters of injection and ignition as well as the combustion process, the research was carried out in the Laboratory for IC engines at the Faculty of Engineering, University of Kragujevac.


KEY WORDS: *alternative fuels, hydrogen, internal combustion engine, injection and ignition parameters*

© 2023 Published by University of Kragujevac, Faculty of Engineering

¹Miroslav Petrović, University of Kragujevac, Faculty of Engineering, Sestre Janjic 6, 34000 Kragujevac, Serbia, petrovickg95@gmail.com, , (*Corresponding author)

²Aleksandar Davinić, University of Kragujevac, Faculty of Engineering, Sestre Janjic 6, 34000 Kragujevac, Serbia, davinic@kg.ac.rs,  <https://orcid.org/0009-0002-0260-3430>

³Nadica Stojanović, University of Kragujevac, Faculty of Engineering, Sestre Janjic 6, 34000 Kragujevac, Serbia, nadica.stojanovic@kg.ac.rs,  <https://orcid.org/0000-0002-4199-0587>

⁴Ivan Grujić, University of Kragujevac, Faculty of Engineering, Sestre Janjic 6, 34000 Kragujevac, Serbia, ivan.grujic@kg.ac.rs,  <https://orcid.org/0000-0003-0572-1205>

UTICAJ PARAMETARA UBRIZGAVANJA I PALJENJA VODONIKA NA PROCES SAGOREVANJA U MOTORU SUS

REZIME: S obzirom da se poslednjih decenija trend upotrtebe vozila povećava, a kako su rezerve nafte ograničene i ekološki zahtevi sve veći, ne preostaje ništa drugo nego da se traže alternativna rešenja kao zamena naftnih derivata. Alternativa su električna vozila i hibridna vozila, ali motore sa unutrašnjim sagorevanjem (SUS) nikako ne treba otpisivati, za OTO motore u upotrebi su alternativna goriva kao što su tečni naftni gas (TNG) i komprimovani prirodni gas (KPG). Postoji još jedno alternativno gorivo za motore SUS koje je još uvek u fazi ispitivanja za primenu na vozilima, a to je vodonik (H_2). O vodoniku kao pogonskom gorivu, još uvek nema mnogo objavljenih rezultata. Ovaj rad će prikazati rezultate dobijene eksperimentalnim istraživanjem na motoru SUS sa vodonikom kao pogonskim gorivom, a rezultati se odnose na parameter ubrizgavanja i paljenja kao i process sagorevanja, istraživanja su vršena u Laboratoriji za motore SUS na Fakultetu inženjerskih nauka Univerziteta u Kragujevcu.

KLJUČNE REČI: *alternativna goriva, vodonik, motor SUS, parametri ubrizgavanja i paljenja*

INFLUENCE OF HYDROGEN INJECTION AND IGNITION PARAMETERS ON THE COMBUSTION PROCESS IN THE IC ENGINE

Miroslav Petrovic, Aleksandar Davinic, Nadica Stojanovic, Ivan Grujic

INTRODUCTION

The key process in the IC engine is the combustion process, the output characteristics of the engine depend on it. The area where most work is done when it comes to engine and fuel development is the optimization of the combustion process flow. The main difference between SI and compress ignition (CI) engines is the way the work process is carried out. The difference in the work processes is reflected in: the way the mixture is formed, the way the mixture is ignited and the regulation of the load. The mixture in the SI engine is formed immediately before entering the cylinder, so that the fresh working material is largely homogenized and consists of fuel vapor and air, and when entering the cylinder it mixes with a small amount of residual combustion products. The ignition of the mixture is carried out forcibly by a foreign ignition source at a precisely determined moment, while the regulation of the load is carried out by changing the amount of fresh working material.

In the SI engine, combustion can be divided into three stages, and these three stages are shown in Figure 1.

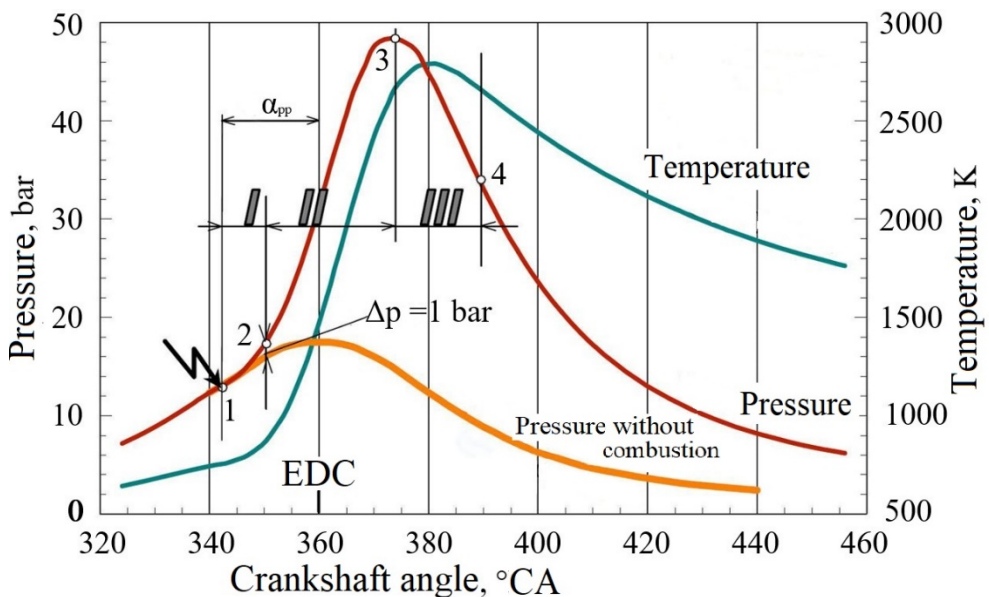


Figure 1. Stages of combustion in SI engines, [1]

The first stage is called the latent combustion period and lasts from the moment the mixture is ignited, by means of a spark between the electrodes of the spark plug, until the pressure increases by 1 bar due to combustion compared to the pressure without combustion. The second stage represents the period of the basic phase of combustion, it lasts until the pressure in the cylinder reaches its maximum value, and during it the turbulent flame has passed the entire volume of the cylinder. The third stage is the burning process.

In the case of CI

engines, the main difference compared to auto engines is reflected in the combustion process, its characteristics are: the operation of the engine with an inhomogeneous mixture, a short time for the formation of the mixture, the combustion process begins before the entire amount of fuel is injected, during one part of the combustion process at the same time both injection and combustion take place. The combustion process in a CI engine is divided into four stages, which is shown in Figure 2.

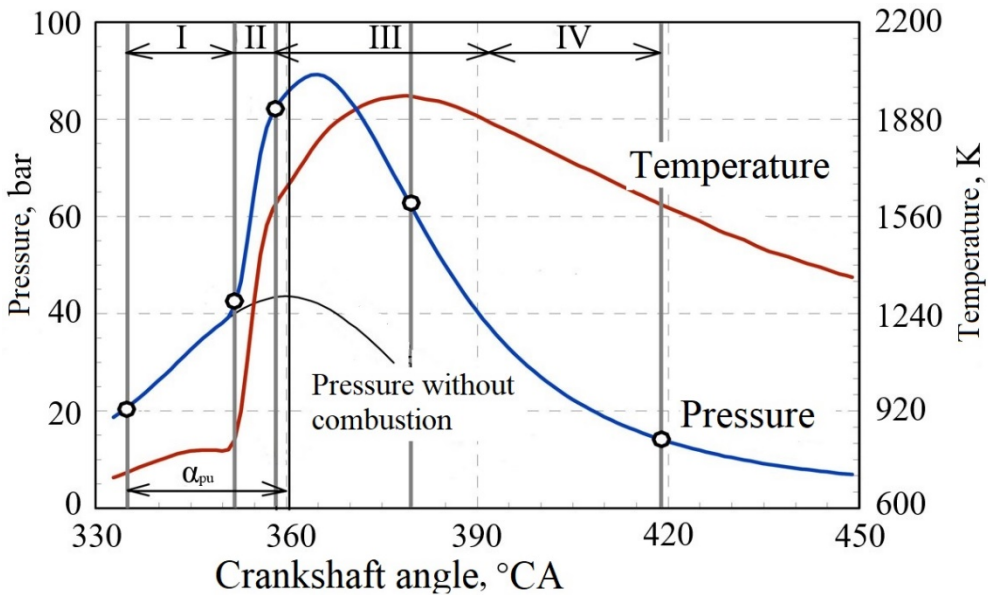


Figure 2. Stages of combustion in CI engines, [1]

The angle of the crankshaft at which the injection starts is called the pre-injection angle, after the start of the injection the physical and chemical preparations for combustion begin, this represents the first stage called the induction period [1]. The second stage consists of a period of uncontrolled combustion, during which rapid combustion occurs, resulting in a large increase in pressure, the tolerance limit for the degree of pressure increase is about $10 \text{ bar} \cdot \text{°CA}^{-1}$. The third stage is the stage of regulated combustion where the law of heat release is proportional to the law of injection. The last or fourth stage of the combustion process is combustion. In this phase, combustion takes place slowly and this phase is extended to the beat of expansion.

The basic variants of IC engines such as SI and CI engines use fuels of fossil origin, i.e. oil derivatives obtained by refining crude oil. As oil is extracted in large quantities, and its production takes a very long time, it is certain that at some point it will disappear. Combustion of fossil fuels releases combustion products that are harmful to human health and the environment. For this reason, the European Union introduced Euro norms, with the aim of protecting the environment. Given that the requirements for environmental protection are constantly increasing, at some point even the latest Euro standards will not be able to satisfy them. Due to all of the above, alternative solutions are being worked on. There are two types of alternative solutions, alternative drive and alternative fuel. Given that there are a very large number of vehicles in the world with conventional engines, the development of

an alternative fuel for use on them stands out as a better solution, and hydrogen stands out as the most promising alternative fuel.

1. OVERVIEW OF RESEARCH IN THE WORLD

Hydrogen is often mentioned as the fuel of the future. There is some research into the application of hydrogen in auto or CI engines. By adding hydrogen, as an additive, in conventional CI engines, harmful emissions of carbon-containing gases are reduced [3], because the chemical composition of hydrogen does not contain carbon. However, due to its high energy, hydrogen raises the maximum temperatures during combustion, which directly affects the increase of nitrogen oxides (NO_x) [3, 4], but it can also affect the reduction of nitrogen oxides as follows [5, 6]:

- exhaust gas recirculation (EGR);

- by adding hydrogen as an additive in the amount of 3.9% of the energy value.

In the case of adding 3.9% of hydrogen, a reduction of 5.5% of nitrogen oxides is achieved [6]. Hydrogen-powered internal combustion engines can operate on a very lean mixture thanks to the wide range of flammability and the high flame speed of the hydrogen-air mixture. A lean mixture reduces the emission of nitrogen oxides and increases the efficiency of the engine. Therefore, the hydrogen engine can operate without or with low damping, which reduces pumping losses and increases efficiency. The first research into the use of hydrogen as a fuel for IC engines indicates that hydrogen is a much better fuel for auto engines. The reason for this is the high self-ignition temperature, which is around 848 K [7]. Using hydrogen as an additive, but in this case with a gasoline engine, also achieves a reduction of toxic components that have carbon in their composition [8]. However, gasoline engines can very easily be modified to run with hydrogen as the only fuel injected into the intake manifold. The biggest problem is the possibility of the flame returning due to the formation of explosive gas (HHO), which ignites very easily. Comparing the performance of the engine when hydrogen or ethanol are added as an additive to gasoline is very difficult [9]. In order to achieve similar or better results with some of the fuels, different pre-ignition angle settings are needed, as well as an accurate calculation of the mixture composition coefficient for the corresponding fuel. Adjusting the preignition angle is critical because of the different burning rates from fuel to fuel.

S. Zanforlin and S. Frigo [10], as part of their research, realized an experimental engine for working with hydrogen as the only fuel. The experimental engine was realized with an unconventional system of two-stage direct injection of hydrogen into the engine cylinder with a low pressure of 6 bar. The system is based on the concept of hydrogen dosing in an intermediate chamber that is separate from the hydrogen inlet valve to the engine. Dosing hydrogen into the intermediate chamber is provided by an electric injector, which can be kept open during the entire engine cycle, so a commercial electric injector for CPG can deliver the required amount of hydrogen even at low pressure. Dosing into the cylinder is done by mechanically starting the injection valve, which, thanks to the sufficient flow section, can be opened for a short time. The injection of hydrogen into the cylinder starts when the intake valves are closed to avoid back-ignition. The layout of the experimental engine from this research is given in Figure 3.

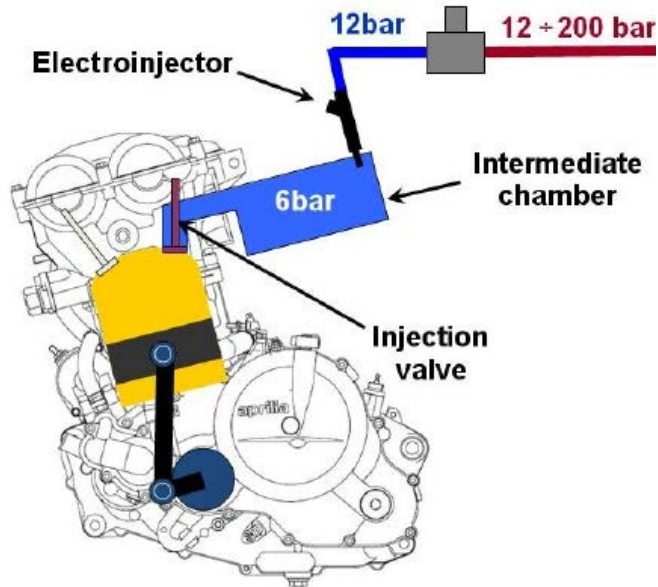


Figure 3. Experimental engine with two-stage direct hydrogen injection, [10]

In short, it can be said that the solution, the sketch of which is shown in Figure 3, combines a system characterized by a constant hydrogen flow rate and a variable opening duration (the first step - an electric injector) with a system characterized by a variable hydrogen flow and a constant angular duration (the second step is a valve for engine injection). The essence of the system is that there are always equalized gas flows through the electric valve and through the mechanical injection valve on the engine, which is controlled by the electric injector. In addition to reducing exhaust emissions, hydrogen is considered an interesting fuel from another aspect. Namely, it is known that hydrogen has a significantly higher burning speed compared to other fuels. Therefore, it is considered that the combustion speed will contribute to the combustion at an almost constant volume, thus increasing the efficiency [11, 12]. However, the high speed of combustion is accompanied by a large increase in pressure, as well as an increase in temperature, which, in addition to the mechanical load, also causes an increase in the emission of nitrogen oxides. By adding a small amount of hydrogen to conventional fuels, emissions are improved [13], but more serious changes in emissions require larger amounts or complete replacement of conventional fuel with hydrogen. This approach often causes a significant increase in nitrogen oxides at the expense of the reduction of other harmful components, as well as the occurrence of detonating combustion. In some research, the injection of water along with hydrogen was considered in order to reduce the combustion speed and thus the emission of nitrogen oxides. It was established that adding water reduces the concentration of nitrogen oxides and detonations do not occur, but this approach is also limited as it has a bad effect on the indicator level of usefulness [14-16]. In addition to water, the concentration of nitrogen oxides in an engine where hydrogen has been used as an additive can be reduced by adding water vapor. By using 30% of hydrogen as fuel, from the total volume of fuel, in CI engines and adding 20% of water vapor, the concentration of nitrogen oxides in relation to when using conventional fuel decreases by 22.1%, and the effective power increases by 22.8% [17].

2. EXPERIMENTAL RESEARCH

A successful engine start was achieved with an injection time of 12ms, by dividing the injection into two portions, the injection start of 30% of the total injection time was set at 344°CA, during intake, and the remaining 70% of the total injection was set at 30°CA before EDC. With this type of injection, a large pressure drop occurred when the engine was started, but with an increase in the number of revolutions, the operation of the engine became more stable. The engine is started with an active decompressor until the first signs of combustion appear, otherwise there will be premature ignition and rotation of the engine direction. To avoid this phenomenon during tarding, an electric starter with a higher starting speed should be used.

2.1 Examination of the method of hydrogen injection

After successfully starting the engine, it was concluded that the engine could fully operate without damping. A certain instability, i.e. lack of ignition, was also observed. During operation, a metallic sound was registered, which appeared every time there was a misfire. The metallic sound was found to be coming from the 200 L silencer tank, which is used to allow airflow measurement. It was discovered that there is actually an explosion in the intake line that echoes in the choke tank. The explosions were caused by HHO gas - explosive gas. The explosion in the suction system was caused by the appearance of a pressure wave that prevented suction and the absence of ignition and combustion. The absence of combustion causes a drop in the number of revolutions and the inability to maintain the regime. As the explosions occurred in the intake manifold, they were caused by the portion of fuel injected during intake. By moving this portion of fuel from the suction to the compression stroke, when both valves are closed, this phenomenon completely disappears, and ensures regular engine operation.

The start of the first injection is set at 200°CA before EDC, and the start of injection of the second part of the fuel is set at 30°CA before EDC. The total injection time and ignition timing are the same, only the injected fuel portions are varied, Figure 4.

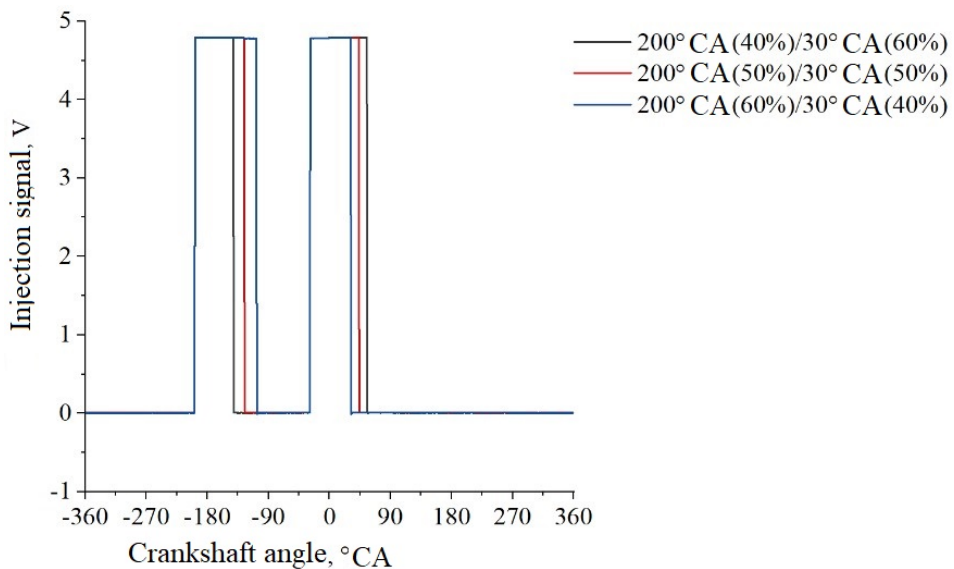


Figure 4. Injection trigger signals for measurements with varying portions of injected fuel

For the first injection method, it is defined that the signal for the first injection lasts 40% and for the second injection 60% of the total injection time. Then, these values were moved to 50% - 50%, and after that to 60% - 40%. During the test, a constant regime was not maintained, but only the influence, redistribution of injection portions was monitored. The headspace pressure for all three measurements is given in Figure 5, and the results in Table 1.

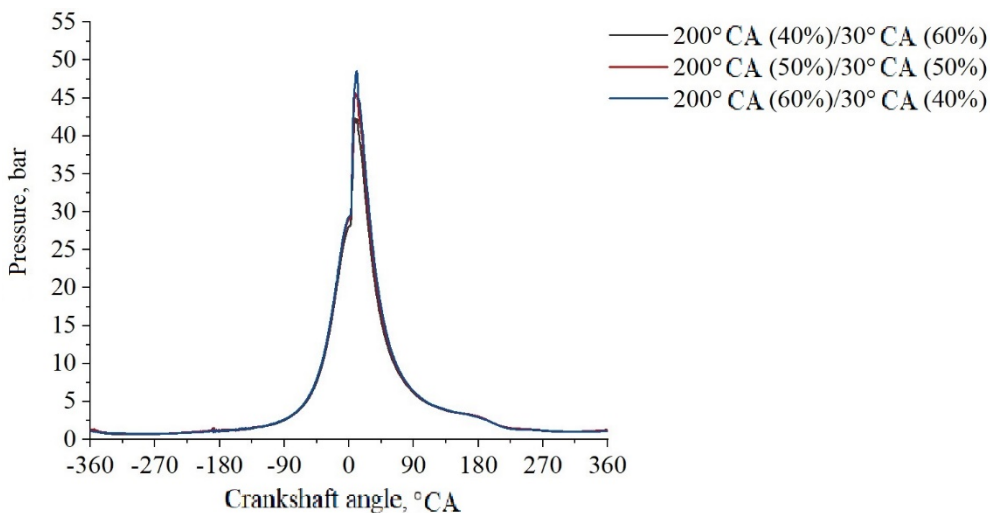


Figure 5. Pressure in the main space for measurements with varying portions of injected fuel

Table 1. Results obtained for measurements with varying portions of injected fuel

Measurements	200°CA (40%)	200°CA (50%)	200°CA (60%)
	30°CA (60%)	30°CA (50%)	30°CA (40%)
Results			
n , min^{-1}	1963	2015	2102
p_{mi} , bar	4,98	5,33	5,67
η_i ,	0,29	0,31	0,34
p_{max} , bar	43,97	48,15	51,19
$\alpha_{p_{max}}$, °CA	8,96	8,50	9,32
$dp/d\alpha$, $\text{bar} \cdot \text{°CA}^{-1}$	6,91	8,66	9,06
AI_{05} , °CA	2,56	2,50	2,56
AI_{10} , °CA	3,37	3,23	3,28
AI_{50} , °CA	8,60	7,53	7,11
AI_{90} , °CA	65,14	60,41	54,62

Labels from the table represent:

- n - number of rotations per minute,
- P_{mi} - mean indicator pressure,
- η_i - indicator degree of usefulness,
- P_{max} - maximum pressure value
- $\alpha_{P_{max}}$ - the position of the maximum pressure value,
- $dp/d\alpha$ - the maximum value of the degree of pressure rise.

Looking at figure 5, it is clearly seen that varying the portions has an effect on the engine duty cycle. With the injection of a larger amount of fuel in the first part of the injection, the maximum pressures in the main compartment increase, as well as the specific indicator work and the indicator degree of usefulness. The differential combustion law for all three modes is shown in Figure 6. With the increase in the amount of fuel injected in the first part of the injection, there is an increase in the maximum value of the heat release rate. The combustion itself is extremely fast, which was to be expected for working with hydrogen, despite the fact that in all three cases the engine worked with a globally lean mixture, with a mixture composition coefficient over 2.

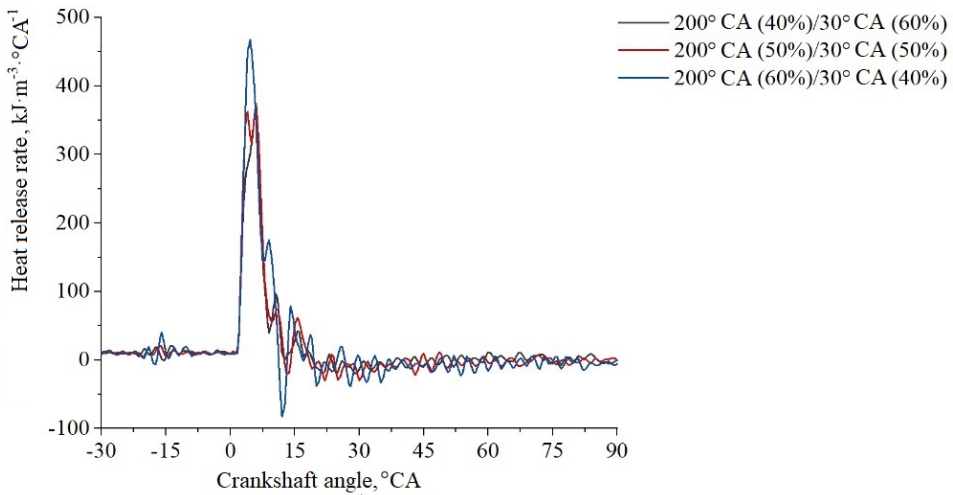


Figure 6. Differential combustion law for regimes with varying portions of injected fuel

2.2 Examination of the hydrogen combustion process

This test was performed on a constant mode defined by the number of revolutions 1570min^{-1} and the load $0.28\text{ kJ}\cdot\text{dm}^{-3}$. This mode did not require a large cycle amount of fuel, which is important both because of the capacity of the injector and because of the limited amount of fuel. At the beginning, it was decided that the injection should be done in two parts. The distribution was adopted such that the injection in each part lasts for 50% of the total injection time. For this test, a constant start of the injection of the first amount at 200°CA before EDC was adopted, which was set as fixed, while the moment of the second injection was varied, shown in Figure 7. Three variants were chosen for the start of the second injection, where two are during compression, and in the third case, the injection starts during

the expansion stroke. In all three cases, the portions per injection are divided into 50% of the total injection time.

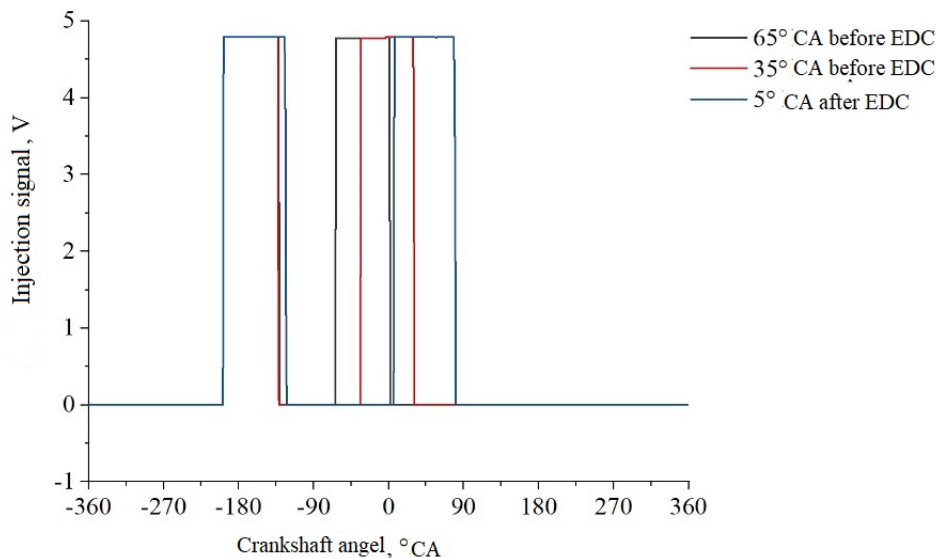


Figure 7. Injection trigger signal for the first three modes

In the research from the previous part, it was shown that the method of injection is an influential parameter, so to maintain a constant mode, the total injection time was changed. The results obtained with this type of injection are shown in Figure 8 and Table 2. It can be seen that with earlier injection, a more violent combustion is achieved, because a larger amount of mixture is successfully formed. This entails higher values of pressures in the main space, as well as higher values of the maximum degree of pressure rise. As for the second portion that occurs during combustion and expansion, its displacement in the direction of expansion has a negative effect on efficiency. The goal was to adopt the best ranking of these three modes based on the results, the first mode can be considered the best, but due to the high degree of pressure increase and the small difference in the indicator level of usefulness between the first and second modes, the second mode was selected for further tests.

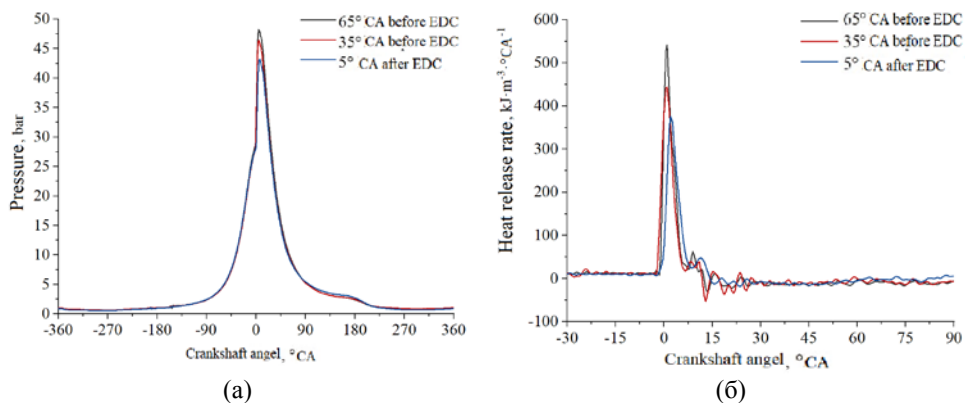


Figure 8. Headspace pressure (a) and differential combustion law (b) for varying the start of injection of the second portion of fuel

Table 2. Results obtained on the regime for varying the start of injection of the second portion of fuel

Measurements	65°CA before EDC	35°CA before EDC	5°CA before EDC
Results			
n, min^{-1}	1581	1562	1561
p_{mi}, bar	5,08	4,77	4,69
$\eta_i,$	0,32	0,31	0,27
p_{\max}, bar	51,11	48,12	44,29
$\alpha_{p_{\max}}, \text{°CA}$	5,82	5,62	6,56
$dp/d\alpha, \text{bar} \cdot \text{°CA}^{-1}$	10,19	7,94	6,48
$AI05, \text{°CA}$	-0,87	-1,48	0,87
$AI10, \text{°CA}$	-0,23	-0,77	1,69
$AI50, \text{°CA}$	2,37	2,23	5,77
$AI90, \text{°CA}$	33,02	45,67	62,55

The next step of the research was to vary the portions per injection. For the adopted injection method (start of injection of the first portion at 200° KV before SMT, and start of injection of the second portion at 35° KV before SMT), shown in Figure 9.

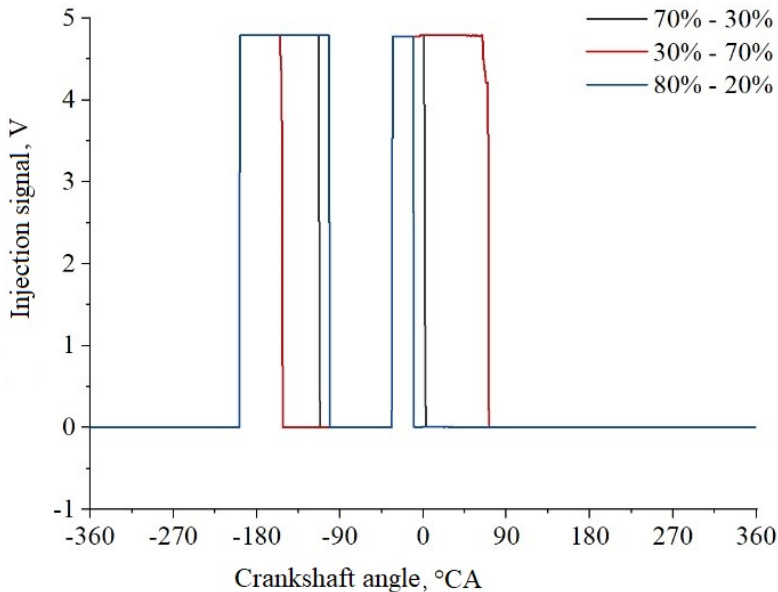


Figure 9. Injection signal for varying the portions of injected fuel

As in the previous case, keeping the regime stable was achieved by redistributing the injection time for the same total injection time. The results obtained with the injection method shown in Figure 9 can be seen in Figure 10 and in Table 3. Injection of a large portion close to the EDC resulted in combustion during the expansion stroke. Since one part of the injection entered the expansion stroke, combustion was caused during the expansion, which is also proven by the angle to which 90% of the cycle fuel was burned. This type of injection led to a decrease in the indicator level of usefulness, and therefore it can be considered that this principle is not favorable from the aspect of efficiency. The other two injection principles, with larger injection portions at the beginning, gave relatively similar results. There was a very short burn in both cases, with the shortest burn recorded at the largest portion of the first injection.

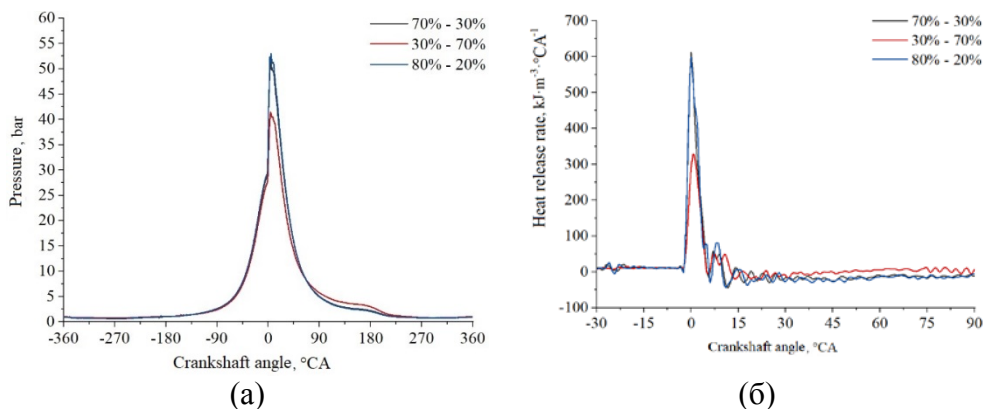


Figure 10. Headspace pressure (a) and differential combustion law (b) for varying fuel injection portions

Table 3. Results obtained on the regime for varying the start of injection of the second portion of fuel

Measurements	70% - 30%	30% - 70%	80% - 20%
Results			
n , min^{-1}	1567	1567	1572
p_{mi} , bar	4,77	4,58	4,78
η_i ,	0,32	0,25	0,33
p_{\max} , bar	53,52	46,62	55,08
$\alpha_{p_{\max}}$, °CA	4,52	4,48	4,34
$dp/d\alpha$, $\text{bar} \cdot \text{°CA}^{-1}$	11,20	6,80	11,21
AI_{05} , °CA	-1,70	-0,52	-1,68
AI_{10} , °CA	-1,10	-0,56	-1,10
AI_{50} , °CA	1,03	8,80	0,99
AI_{90} , °CA	16,93	71,17	8,80

It should be noted that the injection pressure for all shown modes was 100 bar. After the cylinder pressure drop, modes with lower injection pressures were tested, and the injection was successfully moved deeper into the intake stroke. Unfortunately, at lower injection pressures, the cycle amount of fuel also decreases for the same time the injectors are open, and it is not possible to achieve regimes with a higher load. For future research, the possibility of applying the antechamber, especially for working with hydrogen, should not be neglected. However, you need to find a more adequate injector with a larger capacity, which will certainly provide greater engine operation possibilities with this fuel.

3. CONCLUSION

As the need for vehicles is constantly growing, and the requirements for environmental protection are also growing, engineers are under constant temptation to find the best possible solution. Alternative solutions have been developed in the form of alternative drives and alternative fuels. The alternative fuel with the most potential is certainly hydrogen. With hydrogen as a fuel, IC engines can work efficiently with negligible emissions of harmful combustion products, which will surely play a key role in the application of this fuel on vehicles with IC engines.

Experimental studies of engine operation with hydrogen as the only fuel were carried out, injection methods were considered and the combustion process was monitored. It was found that the injection parameters significantly affect the combustion process, and therefore also the operation of the engine. Early hydrogen injection can achieve the best engine performance, although this can lead to unstable operation and excessive mechanical loads on the engine itself, while injection during combustion is not recommended. Injection during combustion does not allow enough time for the mixture to form, which causes stretched combustion and low efficiency. The best solution is injection in two occasions, the first part should be injected during the compression cycle, and the second part around the EDC, injection should be done so that the first portion is significantly larger than the second. This type of injection leads to the enrichment of the mixture at the right moment and slows down combustion..

REFERENCES

- [1] Pešić R., Petković S., Veinović S., *Motorna vozila i motori oprema*, Mašinski fakultet u Kragujevcu, Mašinski fakultet u Banjoj Luci, Kragujevac, Banja Luka, 2008.
- [2] Davinić A., Pešić R., *Pogonski sistemi u transportu*, Fakultet inženjerskih nauka Univerziteta u Kragujevcu, Kragujevac, 2018.
- [3] Pavlos D., Taku T., *A review of hydrogen as a compression ignition engine fuel*; vol. 42, no. 38, *International Journal of Hydrogen Energy*, 2017
- [4] Saravanan N., Nagarajan G., Sanjay G., Dhanasekaran C., Kalaiselvan K.M., *Combustion analysis on a DI diesel engine with hydrogen in dual fuel mode*. vol. 87, no. 17-18, *Fuel*, 2008
- [5] Tsolakis J. A., Hernandez J., Megaritis A., Crampton M., *Dual Fuel Diesel Engine Operation Using H₂. Effect on Particulate Emissions*, vol. 19, no. 2, *Energy & Fuels*, 2005
- [6] Pana C., Negurescu N., Cernat A., Nutu C., Mirica I., Fuiurescu D., *Experimental aspects of the hydrogen use at diesel engine*, vol. 181, *Procedia Engineering*, 2017

- [7] Das L.M., Hydrogen-Oxygen Reaction Mechanism and its Implication to Hydrogen Engine Combustion, vol. 21, no. 8, International Journal of Hydrogen Energy, 1996
- [8] Srinivasana C.B., Subramanian R., Hydrogen as a spark ignition engine fuel technical review., vol. 14, no. 5, International Journal of Mechanical & Mechatronics Engineering IJMME-IJENS, 2014
- [9] Soria A.H.H., Jiménez R.F.E., Morales J.G., Gómez-Aguilar J.F., Pliego T.E.H., Peregrino V.H.O., Theoretical Analysis of the Power of a Spark Ignition Internal Combustion Engine With Different Fuel Blends. The International Conference on Innovative Applied Energy (IAPE'19), 14th-15th March, Oxford, United Kingdom, 2019
- [10] Zanforlin S., Frigo S., Implementation of a novel hydrogen direct-injection concept in single and multi-cylinder engines: CFD, experimental and engine powertrain design studies, vol. 3, no. 1, International Journal of Powertrains, 2014
- [11] Saravanan N., Nagarajan G., An experimental investigation of hydrogen-enriched airinduction in a diesel engine system, vol. 33, no. 6 International Journal of Hydrogen Energy, 2008
- [12] Boretti A., Advances in hydrogen compression ignition internal combustion engines, vol. 36, no. 19, International Journal of Hydrogen Energy, 2011
- [13] Tauzia X., Maiboom A., Shah S.R., Experimental study of inlet manifold water injection on combustion andemissions of an automotive direct injection Diesel engine, vol. 35, no. 9, Energy, (2010)
- [14] Subramanian K.A., A comparison of water–diesel emulsion and timed injection of water into the intake manifold of a diesel engine for simultaneous control of NO and smoke emissions, vol. 52, no. 2, Energy Conversion and Management, 2011
- [15] Ghazal O.H., Combustion analysis of hydrogen-diesel dual fuel engine with water injection technique, vol. 13, Case Studies in Thermal Engineering, 2019
- [16] Adnan R., Masjuki H.H., Mahlia T.M.I., Performance and emission analysis of hydrogen fueled compression ignition engine with variable water injection timing, vol. 43, no. 1, Energy, 2012
- [17] Gonca G., Sahin B., Simulation of performance and nitrogen oxide formation of a hydrogen-enriched diesel engine with the steam injection method, vol. 19, no. 6, Thermal Science, 2015



DEVELOPMENT OF A METHOD FOR DEFINING THE TORSIONAL STIFFNESS OF THE FRAME IN THE INITIAL PHASE OF DESIGNING A HEAVY MOTOR VEHICLE

Miroslav Demić^{1*}

Received in October 2023

Accepted in December 2023

RESEARCH ARTICLE

ABSTRACT: The conceptual design represents the first concretization of the project task, and its main goal is to define the parameters of the driver's ergo-sphere, external dimensions, weight, and performance of the heavy motor vehicle, as well as its stylistic indicators, necessary for further work on the project.

As is known, the parameters of the frame are not known in the initial phase of designing a heavy motor vehicle, so in this paper, an attempt was made to define the required torsional stiffness of the frame based on its transverse vibrations. For this purpose (with the introduced hypothesis), a simplified geometric, physical, and mathematical model of the frame was used, whose random transverse vibrations will be analyzed using some methods of mathematical statistics and the three-variable Fourier transformation.

KEY WORDS: *Heavy motor vehicle, frame, transverse vibrations, torsional stiffness, three-variable Fourier transform*

© 2023 Published by University of Kragujevac, Faculty of Engineering

¹*Miroslav Demić, I Serbian Academy of Engineering Sciences, Kraljice Marije 16, room 218/a, 11000 Belgrade, Serbia, demic@kg.ac.rs, <https://orcid.org/0000-0003-2168-1370>*
(*Corresponding author)

PRILOG RAZVOJU METODE ZA DEFINISANJE TORZIONE KRUTOSTI OKVIRA U FAZI IZRADE IDEJNOG PROJEKTA TERETNOG MOTORNOG VOZILA

REZIME: Idejni projekat predstavlja prvu konkretizaciju projektnog zadatka, a osnovni cilj mu je definisanje parametara ergosfere vozača i spoljašnjih dimenzija, masa i performansi teretnog vozila, kao i njegovih stilskih pokazatelja, neophodnih za dalji rad na projektu.

Kao što je poznato, parametrii okvira nisu poznati u početnoj fazi projektovanja teretnog vozila, pa je, u ovom radu učinjen pokušaj definisanja potrebne torzione krutosti okvira, na bazi njegovih poprečnih vibracija. U te svrhe (uz uvedenu hipodezu) je korišćen uprošćeni geometrisjki, fizički i matematički model okvira, čije će slučajne poprečne vibracije biti analizirane uz korišćenje nekih metoda matematičke statistike i i troparametarska Furijeova transformacija..

KLJUČNE REČI: *Teretno vozilo, okvir, poprečne vibracije, torziona krutost troparametarska Furijeova transformacija*

DEVELOPMENT OF A METHOD FOR DEFINING THE TORSIONAL STIFFNESS OF THE FRAME IN THE INITIAL PHASE OF DESIGNING A HEAVY MOTOR VEHICLE

Miroslav Demić

INTRODUCTION

A heavy motor vehicle defined by the project task is developed in further design phases, where creative and intuitive approaches that played a significant role in the project task development give way to logical and objective factors, calculations, measurements, shaping, evaluations of production and technological capabilities, etc. [1,2].

The conceptual design represents the first concretization of the project task, and its main goal is to define the parameters of the driver's ergo-sphere and the external dimensions, mass, and performance of the cargo vehicle, as well as its stylistic indicators necessary for further work on the project [1,2] heavy motor vehicle.

This paper will discuss the development of a method for defining the torsional stiffness of the frame based on its transverse vibrations. Therefore, the hypothesis is introduced: "Transverse vibrations of the vehicle frame can be used as a parameter for defining torsional stiffness if their quantitative values do not change drastically across the frame's surface, in case of rigorous disturbances (forces, torques)".

The assumption is that the project task defines the need to design a heavy motor vehicle for the market with a total mass of 11,000 kg and a payload capacity of 4,000 kg, with dimensions (length * width * height, mm): 6400 * 2500 * 3600, with a short cab. The engine is positioned at the front, and the vehicle has all-wheel drive.

The designed vehicle must withstand rigorous operating conditions. Other parameters are not mentioned here because they are not of particular importance for defining the torsional stiffness of the frame or investigating its transverse vibrations. For illustration purposes, Figure 1a shows the silhouette of the heavy motor vehicle defined by the project task [1].

Based on the analysis of existing analogous vehicles and the requirements regarding the dimensions of the newly designed vehicle, it was assessed that the frame length could be 6100, mm, and its width 800, mm. The structure would be ladder-type, as shown in Figure 1b) for illustration purposes [3,4].

The dimensions of the corresponding frame profiles should be determined based on their flexural and torsional stiffness. It is emphasized that in practice, an approximate relationship between the stiffness of the springs and the torsional stiffness of the frame is defined [1]. However, since the parameters of the vehicle suspension system are not known in this design phase, the desired torsional stiffness of the frame cannot be precisely defined...

Therefore, it was deemed appropriate to calculate the equivalent height of the frame for the analysis of transverse vibrations based on the mass balance. Namely, it is recommended in [1,2] that the frame of the vehicle should account for 11-15% of its mass. Since it is a lighter heavy motor vehicle, it will be assumed that this share is 12%, which means that the mass of the frame is 840 kg. Bearing this in mind, the following text will discuss the possibilities for analyzing the vibrations of the vehicle frame in this design phase.

1. METHOD

As already mentioned, the concept of a frame and its length and width have been adopted. Now, based on the required torsional stiffness of the frame, it is necessary to define the dimensions of the longitudinal and transverse profiles using some calculation methods, most commonly finite element methods [5,6]. However, as mentioned before, the bending and torsional stiffness, as well as precise external loads, are not known in this design phase, so the application of the mentioned method is not possible with satisfactory reliability.

Considering the aforementioned, as well as the introduced hypothesis, it was deemed appropriate to develop a procedure based on the analysis of transverse vibrations of the vehicle frame. It should be noted that in this design phase, a large number of frame parameters are unknown, so some of them must be obtained through the study of simpler models. It was considered appropriate to idealize and observe the frame as a homogeneous plate of the adopted length and width, with an unknown thickness [7], as shown in Figure 1c). The plate undergoes transverse vibrations under the influence of disturbing forces at the connection points of aggregates, and systems to the frame.

Since the length and width of the frame have been adopted, it is necessary to define the plate thickness based on which the required torsional stiffness of the frame will be calculated. Assuming that the frame is made of steel, the problem was solved by calculating the equivalent plate thickness of 23, mm based on its mass.

To analyze the transverse vibrations of the frame model, it was necessary to define dynamic excitations. Considering that not all excitations are known in this project phase (uneven engine operation, road irregularities, tire non-uniformity, etc.), it was deemed appropriate to analyze vibrations under conditions of short-term intensive braking [8,9]. Based on experience, an impulse shape was chosen with the presence of random changes, as illustrated in Figure 1d).

For further analysis, it was adopted that the engine is supported by the frame at four points, and the cabin is also supported at four points [1]. The cargo box is supported at eight points, but for the sake of simplifying the problem, it is assumed that it is attached to the frame at four points. As for the springs, each of them is connected at two points, but for the same reasons as the cargo box, it is assumed that they are connected at one point each [1]. The illustration of the connecting points is shown in Figure 1d), and the empirical coordinates of the connecting points are given in Table 1.

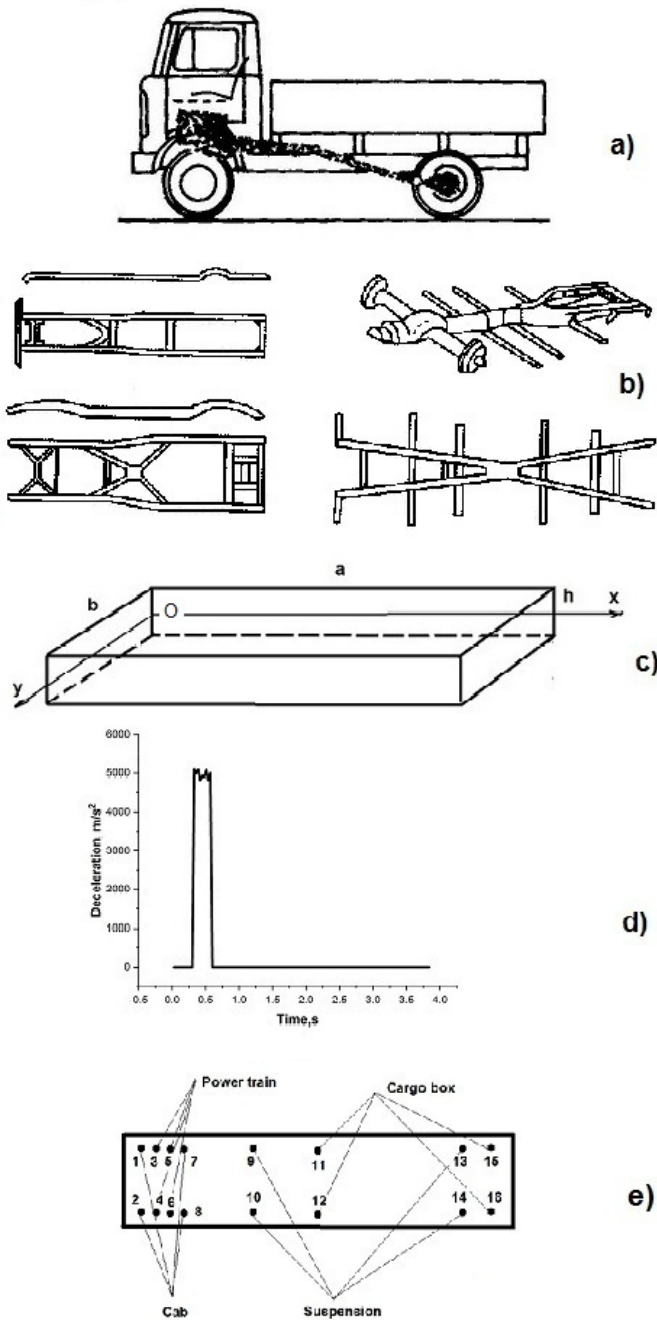


Figure 1. Sketch of the newly designed vehicle a), most commonly used structural solutions for the vehicle frame b), assumed deceleration during vehicle impulse braking c), and equivalent connection points

Table 1. Coordinates of connecting points

	Coordinate x, mm	Coordinate y, mm
1	365	40
2	365	760
3	560	40
4	560	760
5	1375	40
6	1375	760
7	1496	40
8	1496	760
9	1600	40
10	1600	760
11	3400	40
12	3400	760
13	5015	40
14	5015	760
15	5050	40
16	5050	760

To determine the driving forces, it was necessary to calculate the characteristic masses of the aggregates. This was done using statistical data on the percentage participation of aggregate masses in the vehicle mass, as well as based on recommendations on the size of the supported mass [1,2,8,9].

In addition to the mass of the aggregates and systems, it was necessary to calculate the distance between the supports along the length of the vehicle frame (which was done using data from Table 1) and define the height of the aggregate's center of gravity relative to the upper edge of the frame [1]. Approximate data is given in Table 2.

Table 2. Longitudinal distance of connecting points, the height of the center of gravity relative to the frame, and mass of aggregates and systems

	Distance, mm	Height of center of gravity, mm	Mass, kg
Power train	1010	200	962
Cab	1040	800	578
Cargo box	1915	850	890
Suspended mass	3600	1200	8070

Inertial force due to braking is given by the expression [7,8]:

$$F_i = m_i a, \quad (1)$$

where:

- a - acceleration defined by Figure 1d),
- m_i - corresponding mass (powertrain group, cabin, cargo box, suspended mass).

We will assume that the center of gravity of the aggregate and system is located at the midpoint of the longitudinal distance, so in that case, the static load (F_{st}) is equal on all supports and amounts to one-fourth of the gravitational force. The static force increases on

the front supports and decreases on the rear supports during vehicle braking. The magnitude of the force change due to braking is given by the expression [8,9]:

$$\Delta Z = \frac{F_i h_{ii}}{4L_i}, \quad (2)$$

where:

- F_i - inertial force due to braking, defined by expression (1),
- h_{ii} - height of the center of gravity of the corresponding mass from Table 2,
- L_i - longitudinal distance between supports from Table 2,
- + refers to the front supports, and - refers to the rear supports.

Based on expressions (1 and 2), the force on each support is calculated [8,9]:

$$F = F_{st} \pm \Delta Z, \quad (3)$$

Transverse vibrations of the elastic plate are described by a partial differential equation.

The following assumptions were made during its evaluation [7,10]:

- the thickness of the plate is small compared to its dimensions,
- the mid-plane of the plate does not deform and remains as the neutral plane after deformation or bending,
- displacements of the mid-surface of the plate are small compared to the thickness of the plate,
- the influence of transverse shear deformation is neglected, resulting in the fact that the planes normal to the mid-surface before deformation remain normal to the mid-surface even after deformation or bending,
- transverse normal deformation can be neglected under transverse loading, as well as the corresponding stress,
- the cross-section of the frame is rectangular and constant along its length, and
- the material of the frame is homogeneous.

Since the evaluation of the partial differential equation describing the transverse vibrations of an elastic plate is detailed in [7], it will not be done here, but only its final form will be presented.

Based on the introduced assumptions, the forced transverse vibrations of the plate are described by the partial differential equation [7]:

$$D\left(\frac{\partial^4 u}{\partial x^4} + 2\frac{\partial^4 u}{\partial x^2 \partial y^2} + \frac{\partial^4 u}{\partial y^4}\right) + \rho h \frac{\partial^2 u}{\partial t^2} = f(x, y, t), \quad (4)$$

where:

- $u = u(x, y, t)$ - transverse vibrations of the frame,
- x - coordinate along the length of the frame,

- y - coordinate along the width of the frame,
- $f(x, y, t)$ - disturbance transverse force (excitation function),
- t - time.

The value of D is given by the expression:

$$D = \frac{Eh^3}{12(1-\nu^2)}, \quad (5)$$

where:

- E - Young's modulus,
- ν - Poisson's ratio, and
- h - plate thickness.

As known [7,10,11], to find the general solution of the partial differential equation (4), it is necessary to know the boundary and initial conditions.

In this specific case, all edges are free (moments and shear forces are equal to zero), and the vibrations and their velocities are equal to zero at the initial moment [7].

Mathematically, these conditions are defined by the equations:

$$\begin{aligned} M_x &= -D\left(\frac{\partial^2 u}{\partial x^2} + \frac{\partial^2 u}{\nu \partial y^2}\right) = 0; x = 0 \\ V_x &= Q_y - D\left[\frac{\partial^3 u}{\partial x^3} + (2-\nu)\frac{\partial^3 u}{\partial x \partial y^2}\right]; x = 0; Q_y = 0 \\ M_x &= -D\left(\frac{\partial^2 u}{\partial x^2} + \frac{\partial^2 u}{\nu \partial y^2}\right) = 0; x = a \\ V_x &= Q_y - D\left[\frac{\partial^3 u}{\partial x^3} + (2-\nu)\frac{\partial^3 u}{\partial x \partial y^2}\right]; x = a; Q_y = 0 \\ M_y &= -D\left(\frac{\partial^2 u}{\partial y^2} + \nu \frac{\partial^2 u}{\partial x^2}\right) = 0; y = 0 \\ V_y &= Q_x - D\left[\frac{\partial^3 u}{\partial x^2 \partial y} + (2-\nu)\frac{\partial^3 u}{\partial y^3}\right]; y = 0; Q_x = 0 \\ M_y &= -D\left(\frac{\partial^2 u}{\partial y^2} + \nu \frac{\partial^2 u}{\partial x^2}\right) = 0; y = b \\ V_y &= Q_x - D\left[\frac{\partial^3 u}{\partial x^2 \partial y} + (2-\nu)\frac{\partial^3 u}{\partial y^3}\right]; y = b; Q_x = 0 \\ u(x, y, 0) &= 0 \\ u'(x, y, 0) &= 0. \end{aligned} \quad (6)$$

The disturbance force represents the sum of dynamic forces at the supports, i.e.:

$$f(x, y, t) = \sum_{i=1}^{16} F_i(t), \quad (7)$$

where the force $F_i(t)$ is defined by the expression (3) calculated at each support.

The integral of the partial differential equation (4), with the boundary, initial conditions (6), and disturbance force (7), can only be sought in the case of harmonic excitation (and not without difficulties), so an attempt was made to solve it using the Wolfram Mathematica 13.2 software [11]. However, this software allows solving partial differential equations up to the second order, so the problem had to be solved numerically [12] using the finite difference method.

The author developed software for solving the partial differential equation (4) using the finite difference method, with boundary, initial conditions (6), and disturbance force (7), in Pascal. It should be noted that in the case of numerical solving of partial differential equations, sometimes it is necessary to introduce additional boundary and initial conditions [11]...

The dynamic simulation was performed for a steel frame structure with the following data: $E=2.1 \cdot 10^5$, N/mm²; $\rho = 8 \cdot 10^{-6}$, kg/mm³; $\nu = 0.3$; $n_x=128$; $n_y=128$; $n_t=128$; $h_x=47.65$, mm; $h_y=6.25$, mm; $h_t=0.03$, s.

Since the transverse vibrations of the frame depend on three parameters, it is necessary to apply 4D graphics for their graphical representation, which is associated with great difficulties. Therefore, for illustration purposes, partial results for the center of gravity planes: xOt ($y=\text{const}$) and yOt ($x=\text{const}$) are shown in Figures 2 and 3, as it was possible to do using commercial 3D graphics.

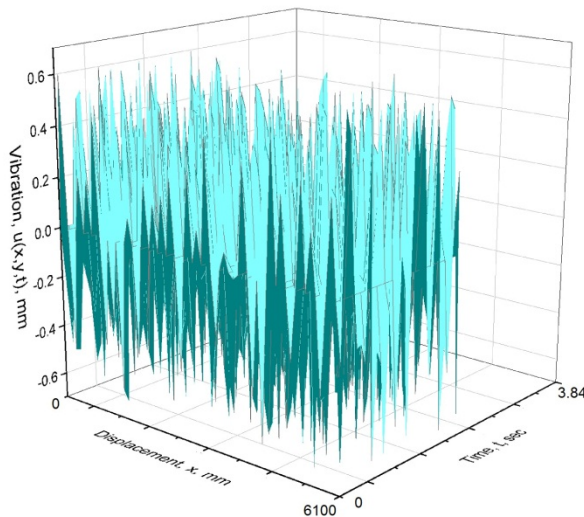


Figure 2. Transverse vibrations of the truck frame in the longitudinal center of gravity plane (xOt)

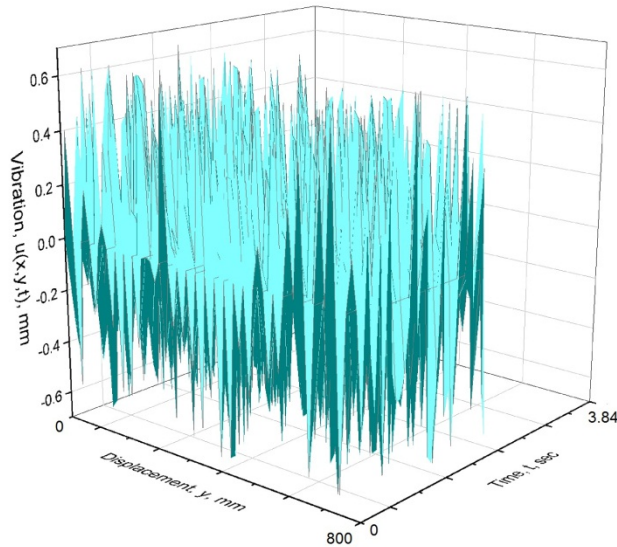


Figure 3. Transverse vibrations of the truck frame in the lateral center of gravity plane (yOz)

Due to the limitations imposed by 3D graphics, the results are partially shown only for the center of gravity of the frame. It was deemed appropriate to calculate the RMS values of vibrations for points with coordinates: 5, 50 and 95% of the length, and 5, 50, and 95% of the width of the frame, for further analysis. The obtained results are shown in Table 3.

Table 3. RMS transverse vibrations at characteristic points of the frame

Coordinates (%*a; %*b): a-length, b-width	RMS* 10^{-1} , mm
5 ; 5	3.661
5 ; 95	3.809
50 ; 5	3.839
50 ; 95	3.787
95 ; 5	3.818
95 ; 95	3.885

For a more detailed analysis of the transverse vibrations of the vehicle frame, it was deemed appropriate to perform a frequency analysis [13-16]. Since the transverse vibrations of the used frame model depend on three parameters (coordinates x , y , and time t), it is obvious that a three-variable Fourier transform must be performed [11,13-16], and based on it, the magnitudes and phase angles of the spectrum are calculated.

The author developed software for calculating the 3D Fourier transform and parameters of the mentioned spectrum in Pascal. Using that software, the magnitudes and phase angles of the 3D Fourier transform were calculated.

It should be noted that the spectra, in this case, depend on three parameters (frequency in x direction, frequency in y direction, and frequency in time domain t), which makes their

graphical representation difficult, as it requires 4D graphics. Therefore, it was deemed appropriate to only show the spectra in the longitudinal and transverse center of gravity planes, in Figures 4-6.

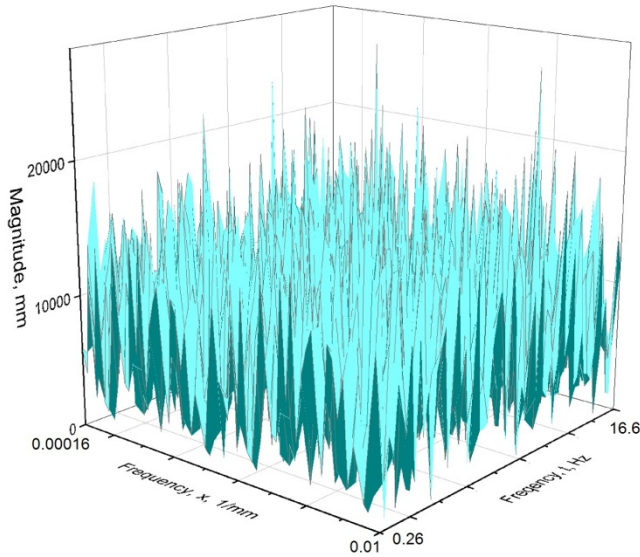


Figure 4. The spectra magnitudes of the heavy motor vehicle frame in the longitudinal center of gravity plane (xOt)

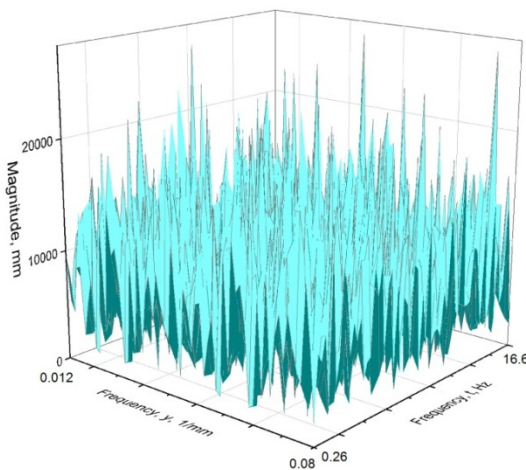


Figure 4. The spectra magnitudes of the heavy motor vehicle frame in the lateral center of Gravity plane (yOt)

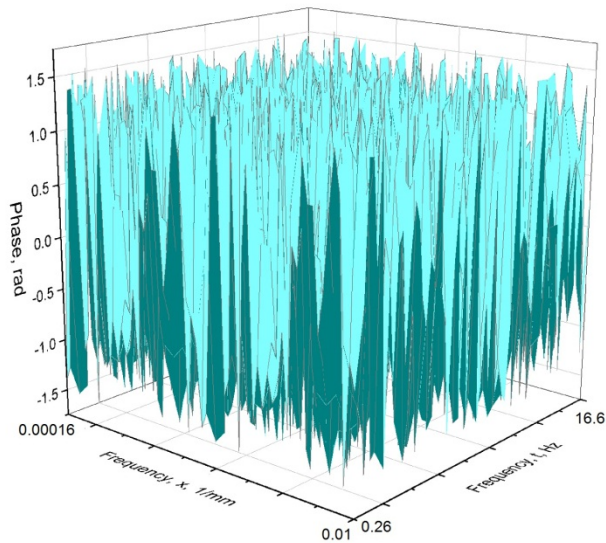


Figure 6. The phase angles of the heavy motor vehicle frame in the longitudinal center of gravity plane (xOt)

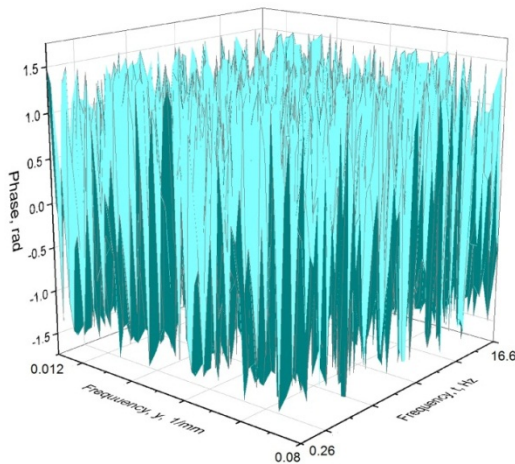


Figure 7. The phase angles of the heavy motor vehicle frame in the lateral center of gravity plane (yOt)

2. DATA ANALYSIS

From Figures 2 and 3, it can be seen that the transverse vibrations for the center of gravity planes of the vehicle frame depend on the position along the length, width, and time. Braking forces are of impact and stochastic nature, which falls into very rigorous conditions in vehicle dynamics [8,9]. More information about the change in vibrations across the surface of the vehicle frame can be found in Table 3.

By analyzing the RMS data from the mentioned table, it can be determined that the transverse vibrations are small (which is desirable from the perspective of vehicle frame

construction) and that the RMS varies across the surface of the observed frame model, which can be explained by the fact that the excitation functions had impact and random characteristics and acted at 16 points. However, these differences are small, indicating that the frame behaves stably under the given conditions, confirming the introduced hypothesis. This allows the defined frame parameters to be used in further frame design. More specifically, the calculated equivalent plate thickness can be used to calculate torsional stiffness, and the used positions of the force application points can serve as guidance for the connection of aggregates and vehicle systems.

From Figures 4-7, it can be observed that random vibrations spread along the length and width of the frame with different amplitudes of modulus and phase angles. This is by the data analysis in the x, z, t space, so there will be no further discussion about it here, and the amplitude and frequency of harmonics depend on the design parameters of the frame and the time excitation...

Considering Parseval's theorem, it was deemed unnecessary to calculate RMS values, as is the case with Table 3.

It should be noted that the number of points and the integration step have ensured the reliability of the results in terms of frequency: x (0.00016 - 0.1, 1/mm), y (0.012 - 0.08, 1/mm), and t (0.26 - 16.6 Hz), which is acceptable from the perspective of frame vibrations in this design phase [18]. In the later stages of the project, when the final structure of the vehicle frame is adopted, research should be conducted with a larger number of points using the finite element method, as existing software allows for automatic mesh generation [19].

It should also be noted that there are no explicit procedures for calculating errors in spectral analysis for 3D Fourier transform, as in the case of 1D Fourier transformation [17]. Bearing this in mind, as well as the fact that this study aims to illustrate the potential of using 3D frequency analysis in investigating transverse vibrations of vehicle frames in the initial design phase, the analysis of statistical errors was not specifically performed...

In the following text, it will be shown how the required torsional stiffness can be calculated based on the defined length, width of the frame, and equivalent plate thickness. Namely, according to [17], there is a known relation that defines the torsional stiffness of a rectangular cross-section:

$$C_t = \beta h b^3 G$$
$$G = \frac{E}{2(1+\nu)}, \quad (8)$$

where:

- E - Young's and Poisson's coefficients (whose values are given in the previous text),
- β - a parameter that depends on the ratio h/b (the value of this parameter is usually defined for ratios greater than 1; since this is not the case for the frame, interpolation should be performed for smaller values, usually linear).

Using equation (8), the required torsional stiffness of the frame can be calculated, which will not be done here.

3. CONCLUSION

The developed procedure, based on the analysis of transverse vibrations of heavy vehicle frames, allows for the determination of the necessary parameters, including torsional stiffness.

The simplified plate-like frame model provides enough opportunities to verify the connection points of the aggregates in the conceptual design phase of the vehicle frame.

In further development of the project, based on the approximately defined parameters of the vehicle frame, more detailed calculations can be performed, potentially using the finite element method.

The conducted analyses have shown that the use of 3D Fourier transformation is useful in analyzing the transverse vibrations of vehicle frames in the initial design phase.

REFERENCES

- [1] Demić, M. (1994) Basics of designing freight motor vehicles", textbook, Faculty of Mechanical Engineering in Kragujevac (in Serbian).
- [2] .Simić, D. (1988) Motor vehicles, Scientific book, Belgrade(in Ser bian).
- [3] Glišović, J., Lukić, J.(2021) Mobile systems, Faculty of Engineering, Kragujevac(in Serbian).
- [4] Janićijević, N. et al. (1991) Construction of motor vehicles, Faculty of Mechanical Engineering, Belgrade (in Serbian).
- [5] Bathe, K.J. (1982) Finite Element Procedures in Engineering Analyses, Prentice Hall, Englewood Cliffs, N.J.
- [6] Ukraincuk, N. (2003) Finite element and finite difference methods, the University of Zagreb, Department of Mathematics (in Croatian).
- [7] Singeresy, S.R. (2007) Vibration of continuous systems, John Wiley and Sons, Inc. New Jersey.
- [8] Genta A. (2003) Motor Vehicle Dynamics, Politecnico di Torino.
- [9] Gillespie T. D. (1992) Fundamentals of Vehicle Dynamics, SAE.
- [10] Sobolev, S. L. (2016) Partial differential equations of Mathematical Physics, Pergamon Student Edition, Elsevier.
- [11] Wolfram Mathematica:
<https://Reference.Wolfram.com/language/tutorial/NDSolverPDE.html>
- [12] Stanton, R. G. (1961) Numerical methods for Science and Engineering, Prentice Hall, Englewood Cliffs, N.J.
- [13] Demić, M. (2023) Contribution to the theoretical-experimental investigation of transverse vibrations of the steering rod of a commercial motor vehicle, *Mobility and Vehicle Mechanics*, Vol 49, No 2, p.p. 27-38.
- [14] Demić, M. (2023)A contribution to the theoretical-experimental investigation of transverse vibrations of the controlling lever of a commercial motor vehicle, *Engineering today*, Online first, DOI: 10.5937/engtoday2300014D.
- [15] Demić, M. (2023) Application of multi-parameters frequency analysis in experimental identification of vibration parameters in motor vehicles, *Mobility and Vehicle Mechanics*, Vol 49, No 1, p.p. 25-37.

- [16] Demić, M. (2023) Contribution to the research of the possibility of application of two-parameter frequency analysis in the experimental identification of torsional vibration parameters of elastic shafts in-vehicle power transmissions, Online first, DOI: 10.5937/engtoday230007D.
- [17] Rašković, D. (1985) Tables of Material Resistance, Construction book, Belgrade
- [18] Bendat, J.S., Piersol, A.G. (2000), Random Data-Analysis and measurement procedures, John Wiley and Sons.
- [19] Software: NASTRAN, ADAMS, CATIA, COSMOS, NASE, SAP, ALGOR, ANSYS, NISA, PAK...



THE STUDY OF THE PROCESSES THAT TAKE PLACE IN GASOLINE INJECTION ENGINES

Vasile Blaga^{1*}, Mihai Blaga²

Received in August 2022

Revised in September 2022


Accepted in October 2022


RESEARCH ARTICLE

ABSTRACT: The fuel supply scheme used to model the system proposed by the authors is presented, the engine chosen, with the technical characteristics, the type of injection system adopted, the basic principle of electronic gasoline injection, the calculation cycle proposed for gasoline injection. Based on an own model, the authors realized an analytical calculation of the in diagram. The indicated diagram was also raised on an experimental stand in p - V coordinates. Using the equations from the characteristic points, the state parameters in the characteristic points of the engine cycle will be calculated. The diagram for the analytical calculation of the pressure in the intake manifold and of the intake pressure is presented; the variation of these parameters is represented depending on the speed and the ambient temperature. The logic diagram for the analytical calculation, determining the engine parameters are presented. The data obtained by calculations are compared with those obtained by measurements, and the results obtained show that the errors obtained are almost insignificant.

KEY WORDS: total displacement, minimum cylinder volume, maximum cylinder volume, compression ratio, dosage, fuel mass, injection duration, indicated diagram.

© 2023 Published by University of Kragujevac, Faculty of Engineering

¹Vasile Blaga, IUniversity of Oradea, Mechanical Engineering and Automotive Department, 1 University Street, Bihor County, Romania, vblaga.ar@gmail.com,  <https://orcid.org/0000-0002-6843-9832>, (*Corresponding author)

²Mihai Blaga, University of Oradea, Mechanical Engineering and Automotive Department, 1 University Street, Bihor County, Romania, mihaibлага332@gmail.com,  <https://orcid.org/0000-0003-1806-2691>

PROUČAVANJE PROCESA KOJI SE ODVIJAJU U MOTORIMA SA UBRIZGAVANJEM BENZINA

REZIME: Prikazana je šema sistema za napajanje gorivom koja je korišćena za modeliranje sistema koji su predložili autori, izabrani motor, sa tehničkim karakteristikama, usvojenim tipom sistema ubrizgavanja, osnovnim principom elektronskog ubrizgavanja benzina, predloženim proračunskim ciklusom za ubrizgavanje benzina. Na osnovu samostalno razvijenog modela, autori su realizovali analitički proračun indikatorskog dijagrama. Navedeni dijagram je određen na eksperimentalnom stolu u p - V koordinatama. Koristeći jednačine iz karakterističnih tačaka, izračunati su parametri stanja u karakterističnim tačkama ciklusa motora. Prikazan je dijagram za analitički proračun pritiska u usisnoj grani i usisnog pritiska; varijacija ovih parametara je predstavljena u zavisnosti od brzine i temperature okoline. Prikazan je algoritam za analitički proračun za određivanje parametara motora. Podaci dobijeni proračunom upoređeni su sa onima dobijenim merenjima, a dobijeni rezultati pokazuju da su dobijene greške gotovo beznačajne.

KLJUČNE REČI: *ukupna zapremina, minimalna zapremina cilindra, maksimalna zapremina cilindra, stepen kompresije, doziranje, masa goriva, trajanje ubrizgavanja, prikazani dijagram*

THE STUDY OF THE PROCESSES THAT TAKE PLACE IN GASOLINE INJECTION ENGINES

Vasile Blaga, Mihai Blaga

INTRODUCTION

The mode of operation of the engine is defined by speed and load, but requires knowledge in addition to these and the thermal regime, ie parts temperature, coolant temperature, air temperature, exhaust temperature, altitude corrections, etc. [3]

It is most often preferred that the opening time of the electromagnetic injector be based on the depression in the intake manifold, as the amount of petrol injected per cycle is correlated with the amount of air drawn in per cycle, the speed dependence in this case being lower, and speed corrections will be made to operating modes that require such corrections.

Corrections to the fuel flow injected into the cylinder are required by a number of transient modes of engine operation, cold start, as well as coolant temperature, cylinder air temperature, lubricating oil temperature, atmospheric pressure. In view of all this, the basic principle expressed graphically in Figure 1 applies to the construction of the injection equipment.

A fuel pump extracts the fuel from the tank and discharges it to the electromagnetic injectors.

The gasoline pressure upstream of the injectors is kept constant by means of a pressure regulator which allows the return of excess gasoline discharged by the feed pump into the tank. [2]

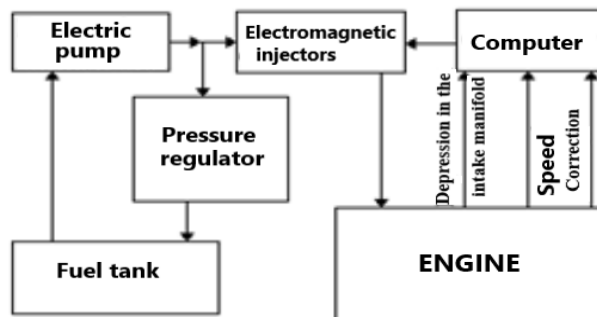


Figure 1. The basic principle of electronic fuel injection

The scheme of the fuel supply system used for the calculus is presented in figure 2.

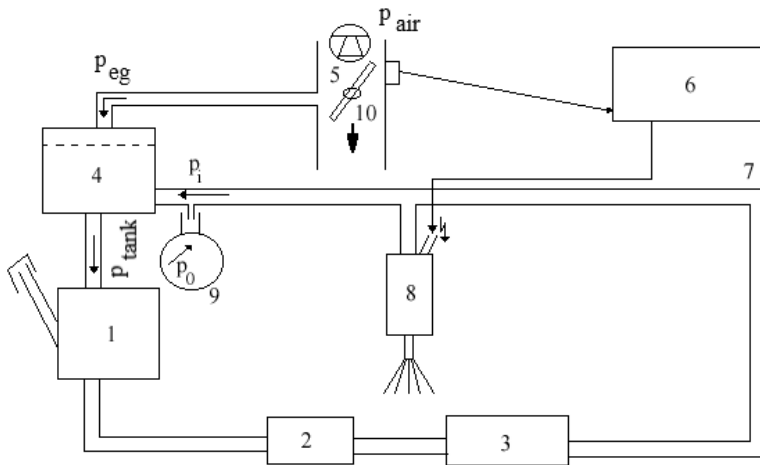


Figure 2. The fuel supply system: 1 – fuel tank; 2 – electric pump; 3 – fuel filter; 4 – pressure regulator; 5 – flow meter to measure the intake air quantity; 6 – computer; 7 – injection manifold; 8 – electromagnetic injectors; 9 – valve to measure the pressure in the system; 10 – throttle; p_{air} – the environmental pressure; p_{eg} – the pressure of the exhaust gases; p_i – the injection pressure; p_{tank} – the pressure in the fuel tank.

The modelling of the SI engine cycle proposed by the authors is realized by running a computer program. The engine cycle proposed by the authors for the analytical calculus is presented in figure 3.[5]

The simplifying hypotheses that allow the definition of this cycle are the following:

- the intake process takes place at a constant pressure p_a , permanently lower than the atmospheric pressure p_o with the value of the pressure losses Δp_a characteristic of the intake process. The intake process begins at point r_1 with the opening of the intake valve OIV and ends at the inner dead center TDC closing of the intake valve CIV;
- the $d-d_1-r$ evacuation process takes place in two stages: after opening the exhaust valve OEV at BDC. the stage of free evacuation $d-d_1$ at constant volume of the gas takes place during which the pressure decreases from p_d to p_r higher than the atmospheric pressure with the value of the pressure losses Δp_r characteristic of the exhaust route. The evacuation at constant pressure p_r step d_1-r follows, which ends with the closing of the exhaust valve CEV;
- the connection between the exhaust valve and the intake valve is made by means of the isentropic expansion $r-r_1$ of the waste gas.
- the $a-c$ compression process of the fresh mixture is assimilated with a constant polytropic exponent $n_c < k_c$ during which the gas yields to the walls of the cylinder the heat H_{pc} ;
- the combustion process is schematized in two evolutions: the isochoric evolution $c-z$ in which the heat input is H_v and the polytropic evolution of exponent $n_u < 1$ which defines the post-firing and in which the agent receives the heat H_u ;

- the expansion process begins with the theoretical completion of the combustion at point u being assimilated with a polytropic of exponent $n_{d1} > k_d$ which leads to the release of heat H_{pd} to the cylinder walls;
- the thermal agent is considered to behave as a perfect gas with specific temperature-dependent heat.

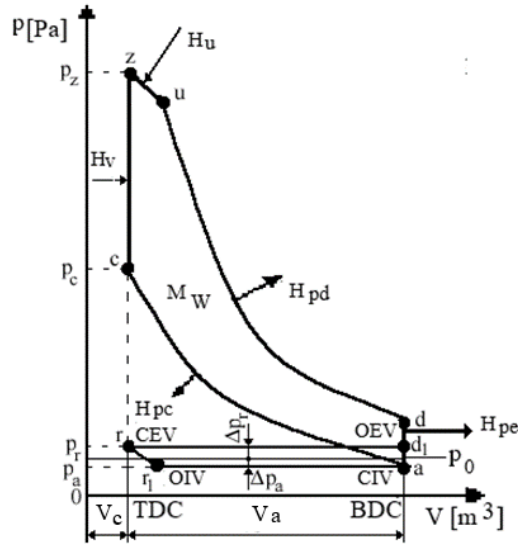


Figure 3. The engine cycle for the analytical calculus [1].

It is emphasized that the assimilation of the post-burning process with a non-subunit exponent polytrope is based on experimental data [5] which show that the final burning temperature T_u is higher than the final burning temperature T_z of constant volume burning c-z, due to an intense release heat on the first z-u portion of the z-u-d process of lowering the gas pressure in the cylinder.

By changing the exponent, the influence of the heat dissipation rate during post-firing cannot be highlighted, on the one hand, and on the other hand, experimental data can be used on the value of the polytropic exponent n_d which characterizes the general expansion of z-u-d gases. In other words, by combining the post-combustion z-u of the exponent $n_u < 1$ and the actual expansion u-d of the exponent $n_{d1} > k_d$, even the actual expansion z-d characterized as is known by a polytropic exponent $1 < n_d < k_d$ is obtained.

The main notations used at the modelling are: $\alpha = p_z/p_c$ – the pressure raise ratio in the isochoric phase of the burning process; $\delta = V_u/V_z$ – the volume raise ratio in the afterburning process; $\varepsilon_1 = V_u/V_z$ – the volume raise ratio during the expansion process; $\psi_0 = \Delta p_a/p_0$ – the relative pressure drop coefficient during the intake process; $\psi_1 = \Delta p_r/p_r$ – the relative pressure drop coefficient during the exhaust process; $\psi = p_a/p_r$ – the global coefficient of the pressure losses; $\varphi_r = T_{d1}/T_r$ – the ratio between the temperature at the end of the forced exhaust and the temperature at the end of the free exhaust.

The initial data for the computation are the following: $D = 77 \cdot 10^{-3}$ m; – the cylinder bore; $S = 83,6 \cdot 10^{-3}$ m; the piston stroke; $V_s = 0,389 \cdot 10^{-3}$ m³; – the swept volume; $R = 290$ J/kg – the working fluid constant; $Q_i = 44 \cdot 10^6$ J/kg; – the net calorific value; $L_0 = 15$ kg air/kg fuel – the stoichiometric air requirement; $T_0 = 293$ K – the environmental temperature; $p_0 = 1 \cdot 10^5$ Pa –

the environmental pressure; $\lambda=1$ – the excess air factor; $\eta_{ar}=0,9$ – the burning process efficiency; $\xi_0=0,8$ – the heat release coefficient; $\xi_{ga}=2$ the gas-dynamic resistance factor of the intake manifold; $\rho_0=1,177 \text{ kg/m}^3$ – the intake air density; $d_0=0,42 \cdot D$ [m] – the inner diameter of the intake manifold at the valve port; $n=500 \dots 5500 \text{ min}^{-1}$ (with a variation from 100 to 100 min^{-1}) – the crankshaft rotational speed; [m/s] – the mean piston speed; $n_u=0,9$ – the polytropic coefficient of the afterburning process; $\eta_p=0,96$ – the plenitude coefficient of the engine cycle; $p_r=1,13 \cdot 10^5 \text{ Pa}$ – the residual exhaust gas pressure (the pressure in point r).

Below is presented the algorithm for the calculation of the state parameters of the working gas in the characteristic points of the engine cycle: point (a) – the end of the intake stroke; point (c) – the end of the compression process; point (z) – the end of the isochoric burning process; point (u) – the end of the afterburning process, point (d) – the end of the expansion process; point (d_1) – the end of the free exhaust process.

The logical scheme for the analytical calculation is presented in figure 8.[5]

The computation program is structured on 10 procedures and functions. In addition to the values of the constants declared at the beginning of the program, one also considers as initial data, assumed known arbitrarily chosen from statistic data of the SI. engine cycle: $T_{a0}=322 \text{ K}$, $T_{z0}=2530 \text{ K}$, $T_{u0}=2660 \text{ K}$, $k_{c0}=1,3$, $k_{v0}=1,3$, $k_{u0}=1,2$, $k_{d0}=1,3$ and $k_{e0}=1,3$. Without these, it is not possible to calculate, generally speaking, all the other parameters that characterize the engine cycle. Thus, this initial data will play the role of parameters, the variables being explicitly the temperature between these thermal processes evolve. These temperatures are closely depending on the adiabatic coefficients which, in fact, are stabilized by the completion for several times of the engine cycle until these coefficients become constant, with an error of 0,000009. The decision for the exit from the cycle for a particular rotational speed is given by the decreasing of the constant error of the intake temperature (T_a) under the value 1,5 K. [5]

1. THE CALCULATION OF THE PRESSURE IN THE INTAKE MANIFOLD p_{ga} AND THE INLET PRESSURE p_a

Considering the intake process, the case when the engine fluid density is variable applies the Bernoulli gas flow equation, written for the inlet section 0-0 and section 2-2 (figure 4). [1]

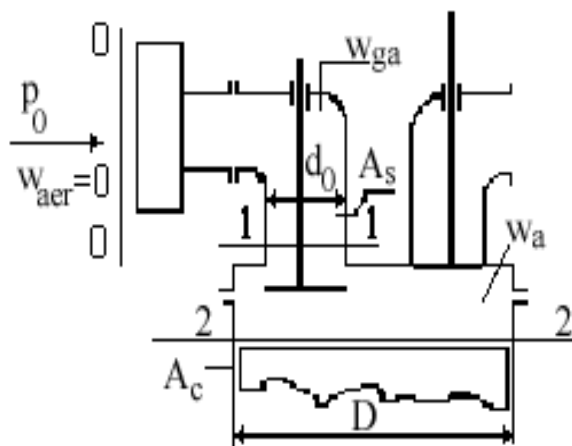


Figure 4. The sketch for the analytical calculation of p_{ga} and p_a

It is written Bernoulli's relation between sections 0-0 and 1-1 to determine the pressure in the intake manifold p_{ga} , and then between sections 0-0 and 2-2, in which case determine the inlet pressure p_a :

The pressure at the intake valve port [3] and [4]:

$$p_{ga} = p_0 - k_1 \left(1 + \xi_{ga}\right) n^2 \left(\frac{V_s}{d_0^2}\right)^2$$

$$k_1 = \frac{1}{1 + 1 + \xi_{ga} \frac{k_a}{2} \left(\frac{4}{30\pi}\right)^2 \left(\frac{V_s^2}{D^2}\right)^2 \left(\frac{n}{a_{sa}}\right)^2}, \tag{1}$$

where:

- a_{sa} [m²] – the effective flow area through the orifice controlled by the intake valve;
- $k_a=1,4$ – the adiabatic exponent of the intake process.

The pressure at the end of the intake stroke [1] and [4]:

$$p_a = p_{ga} - k_1 n^2 \frac{V_s}{d_0^4} \left[\left(1 + \xi_{ga}\right) \left(\frac{d_0}{D}\right)^4 - 1 \right], \tag{2}$$

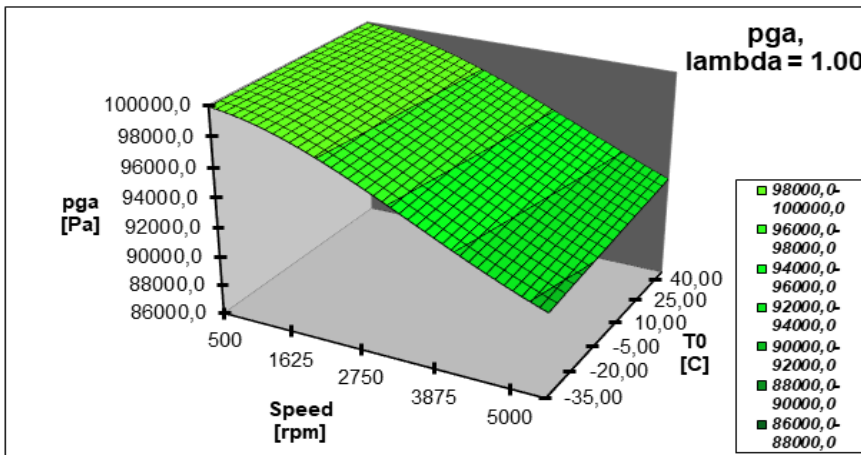


Figure 5. The variation of pressure in the intake manifold with speed and temperature

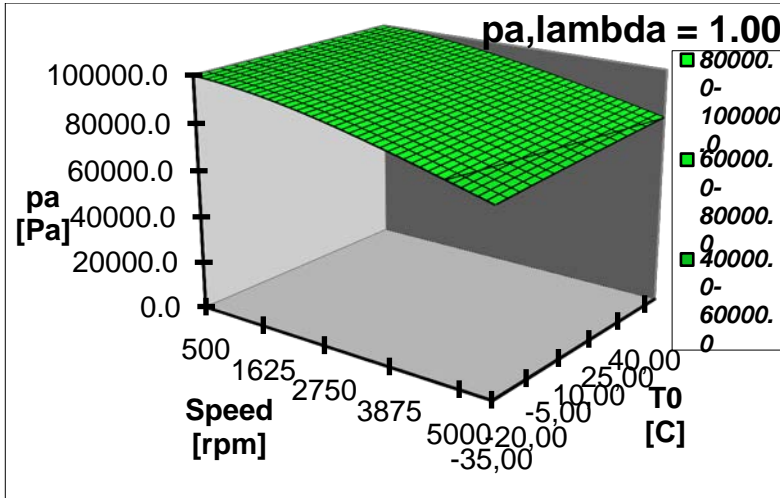


Figure 6. The variation of inlet pressure with speed and ambient temperature

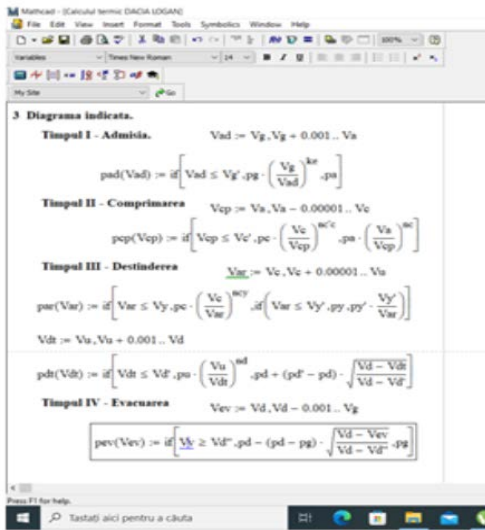


Figure 7. Part of the calculation program

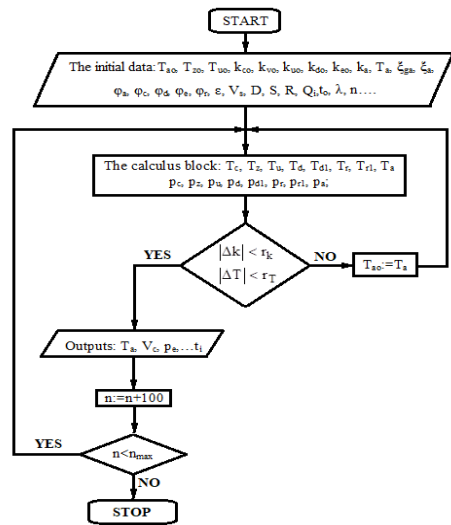


Figure 8. The logical scheme for the calculus

2. THE MODEL CALCULATION FOR CYCLE THERMODYNAMIC DIAGRAM P – V

The mathematics equation for transformation what make the thermodynamics cycle after who run Engines with spark Lightning study are: [7];[8]

2.1 The polytrophic compression a-c:

$$p = p_a \left(\frac{V_a}{V} \right)^2; V \in [V_a; V_c];$$

$$V_a = V_c + V_s = \frac{V_s}{\varepsilon - 1} + V_s;$$
(3)

2.2. The isochors burn c-z:

$$p = \alpha p_c; V = V_c = ct;$$
(5)

2.3. The polytrophic relaxation z-u:

$$p = p_z \left(\frac{V_z}{V} \right)^{n_u}; V \in [V_c; V_u]; V_u = \delta V_c;$$
(6)

2.4 The polytrophic relaxation u-d:

$$p = p_u \left(\frac{V_u}{V} \right)^{n_d}; V \in [V_u; V_d]; V_{d1} = V_a;$$
(7)

2.5 The freely evacuation d-d1:

$$p = p_{d1}; V = V_a;$$
(8)

2.6 The forced evacuation d1-r:

$$p = p_{d1}; V = V_r = V_c;$$
(9)

2.7 The adiabatic extend to evacuation r-r1:

$$p = \left(\frac{V_r}{V_{r1}} \right)^{k_e}; V_{r1} = V_r \left(\frac{p_r}{p_a} \right)^{\frac{1}{k_e}};$$
(10)

2.8 Admissible at constant pressure r1-a:

$$p = p_a; V = V_a;$$
(11)

Table 1. Representation of the entire the spark ignition engine cycle:

The point	pressure [10 ⁵ Pa]	Volume [dm ³]
a	0,8127299	0,43615
c	16,6868451	0,04715
z	54,6920726	0,04715
u	38,4259264	0,06979
d	3,6384934	0,43615
d1	1,14469	0,43615
r	1,14469	0,04715
r1	0,8127299	0,06159

$nciclu := n1 + n2 + n3 + n4 + n5 + n6 + n7 + n8$	
$ic := 1 .. nciclu$	$nciclu = 230$
$p_{i1} := p1_{i1}$	$V_{i1} := V1_{i1}$
$p_{n1 + i2} := p2_{i2}$	$V_{n1 + i2} := V2_{i2}$
$p_{n1 + n2 + i3} := p3_{i3}$	$V_{n1 + n2 + i3} := V3_{i3}$
$p_{n1 + n2 + n3 + i4} := p4_{i4}$	$V_{n1 + n2 + n3 + i4} := V4_{i4}$
$p_{n1 + n2 + n3 + n4 + i5} := p5_{i5}$	$V_{n1 + n2 + n3 + n4 + i5} := V5_{i5}$
$p_{n1 + n2 + n3 + n4 + n5 + i6} := p6_{i6}$	$V_{n1 + n2 + n3 + n4 + n5 + i6} := V6_{i6}$
$p_{n1 + n2 + n3 + n4 + n5 + n6 + i7} := p7_{i7}$	$V_{n1 + n2 + n3 + n4 + n5 + n6 + i7} := V7_{i7}$
$p_{n1 + n2 + n3 + n4 + n5 + n6 + n7 + i8} := p8_{i8}$	$V_{n1 + n2 + n3 + n4 + n5 + n6 + n7 + i8} := V8_{i8}$

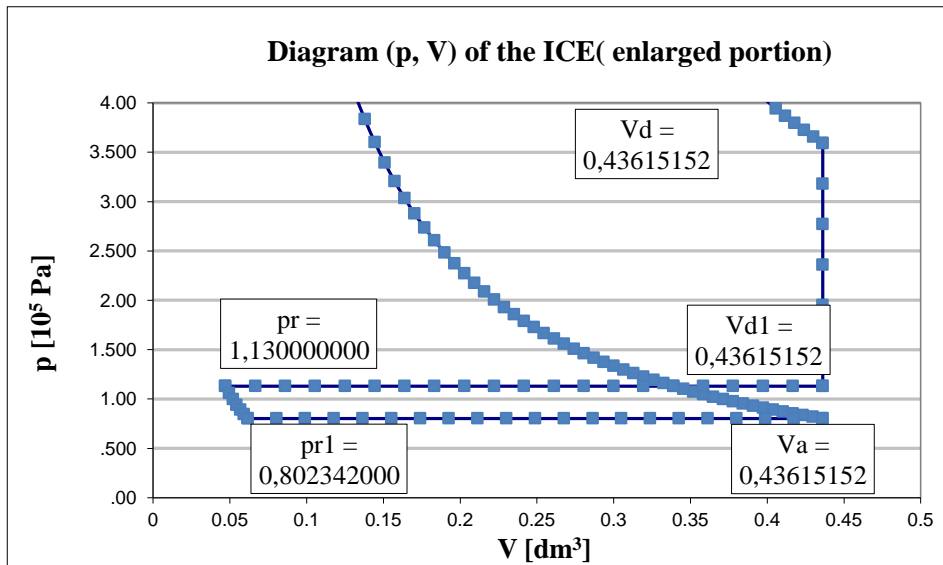


Figure 9. The gas exchange diagram

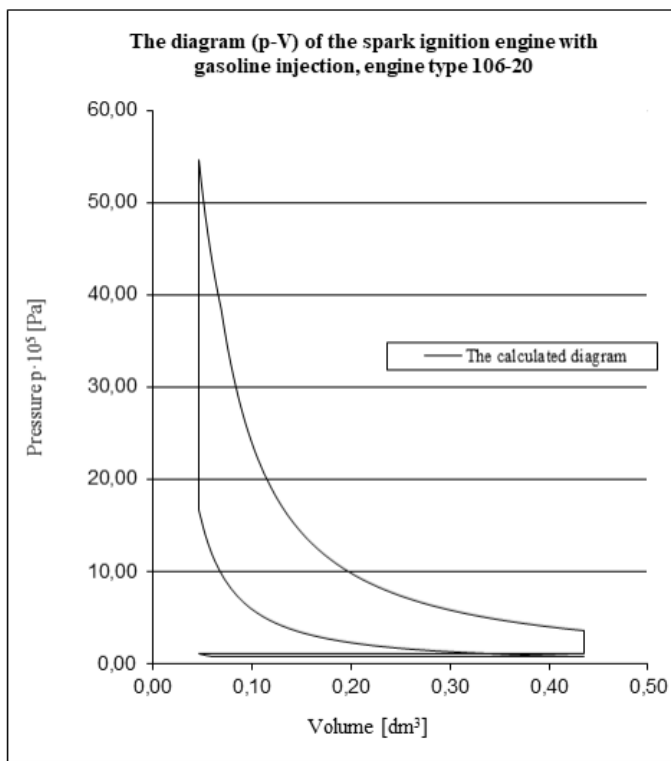


Figure 10. The calculated indicated diagram.

The computation program was realized in Mathcad and part of it is shown in figure 9.

The calculated indicated diagram, obtained with this computer program, is presented in figure 10.

3. THE REAL INDICATED DIAGRAM

The general configuration of a test bed for the measurement of the parameters of a S.I. engine. The test bed on which the experimental data were acquired is provided with an electric machine with eddy currents of a W130 Shenk type. [9]

The data acquisition system sums 32 measurement lines to measure the pressure, the temperature, the rotational speed, the torque, the environmental parameters and so. The data acquisition and processing are automatically made by using a processes computer that is provided with a set of programs necessary for the execution of the set of especially programs to emit the commands necessary to execute the probs included in the testing procedures and for the automatic processing of the data recorded during the testing.

The transducers and the experimental devices are of:

- a resistive type – their verification was made with testers to verify the resistance depending on the cooling liquid temperature and on the intake air temperature;
- an inductive type, in which a magnetic field created by a permanent magnet has a good magnetic conductivity.

The variation of the magnetic field induces in the electromagnetic coil an electric current of voltage (V), that is directed through a cable to the electronic command unit. The setup of the test bed is presented in figure 11.



Figure 11. The test bed used to obtain the indicated diagram.

The pressure inside the cylinder was measured using a pressure sensor for combustion analysis AVL GH 14 DK. Its characteristics are presented in figure 12.



Specifications		
Measuring range	0...300 bar	
Overload	350 bar	
Lifetime	≥ 10 ⁸	load cycles
Sensitivity	19 pC/bar	nominal
Linearity	≤ ± 0.3%	FSO
Natural frequency	~ 170 kHz	
Acceleration sensitivity	≤ 0.0005 bar/g	axial
Shock resistance	≥ 2000 g	
Insulation resistance	≥ 10 ¹³ Ω	at 20 °C
Capacitance	7.5 pF	
Operating temperature range	-40 ... 400 °C	
Thermal sensitivity change	≤ 2 %	20 ... 400 °C
	≤ ± 0.5 %	250 ± 100 °C
Load change drift	1.5 mbar/ms	max. gradient
Cyclic temperature drift *	≤ ± 0.7 bar	
Thermo shock error **		
Δp	≤ ± 0.4 bar	
Δp _{min}	≤ ± 2 %	
Δp _{max}	≤ ± 1.5 %	
Thread diameter	M5x0.5	front sealed
Cable connection	M4x0.35	negative
Weight	2.2 grams	without cable
Mounting torque	1.5 Nm	

*) at 7 bar IMEP and 1300 rpm, diesel
 **) at 9 bar IMEP and 1300 rpm, gasoline

Figure 12. The pressure sensor used for tests and its characteristics

4. TEST SCHEDULE

The object Engine type: 106-20

Features: 1557 cm3 tranverse plasament motors ε= 9,25 supply/ignition with Bosch Mono-Motronic M.A. 1.7

The purpose:

Contributions to gasoline injection molding on 106-20 type engine. Definition of injection timing and ignition advance maps and correction charts function to ensure the dryveability of cars.[5]

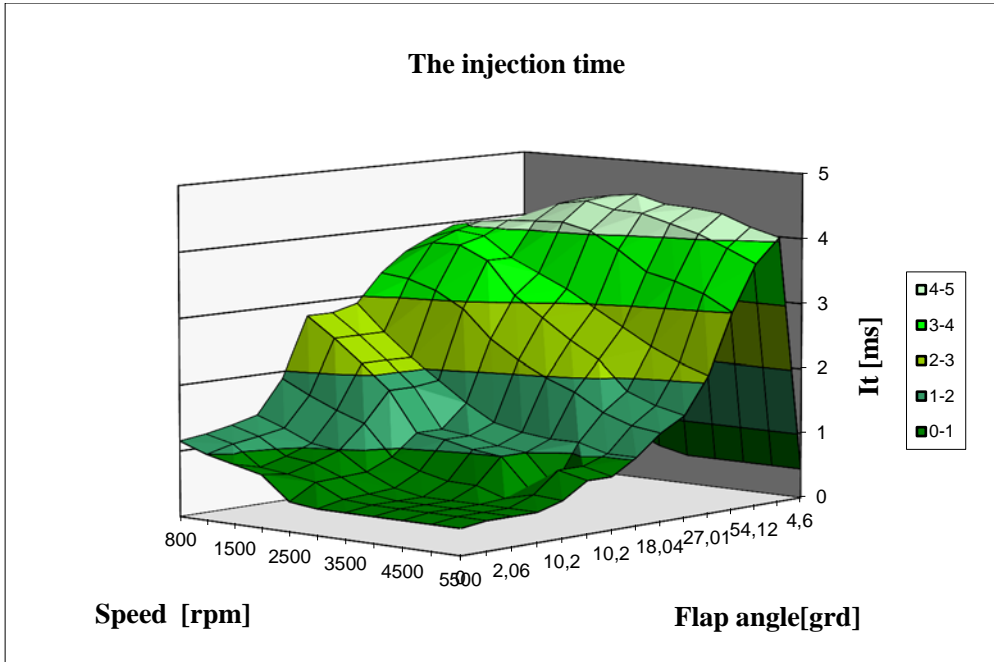


Figure 13. The injection duration cartography

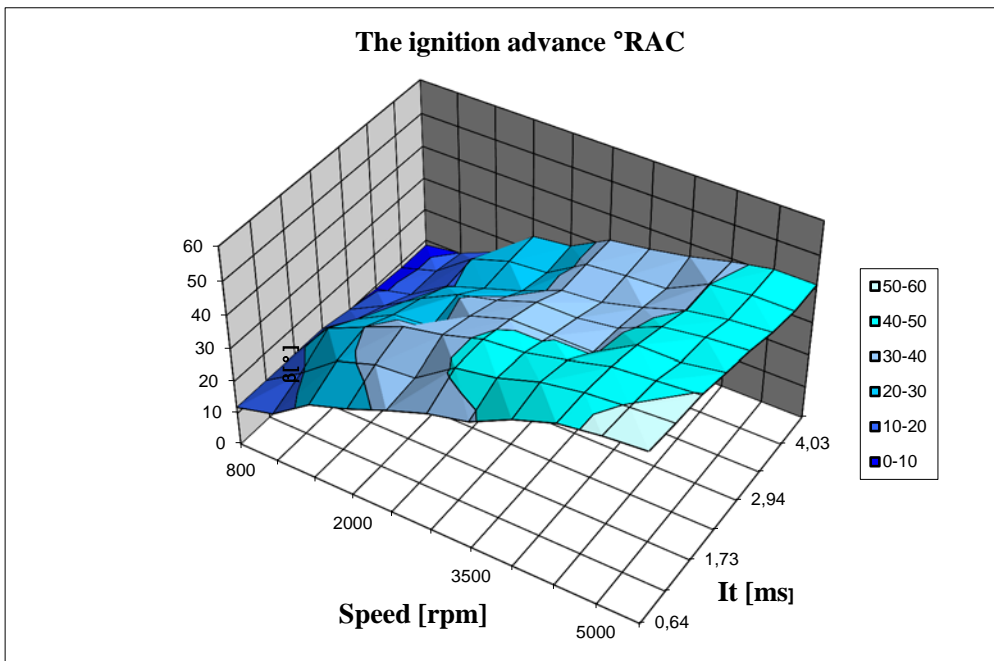


Figure 14. The ignition advance cartography

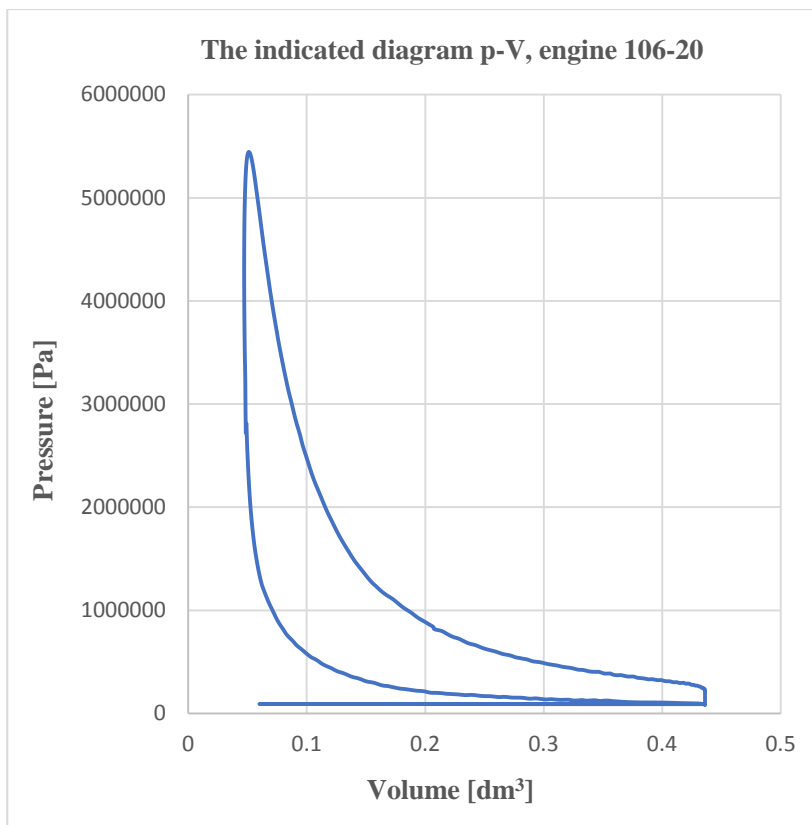


Figure 15. The real indicated diagram

5. CONCLUSIONS

The model for gasoline injection system was proposed, the author used the Bosch Mono-Motronic M.A.1.7 system, adapted to the engine of the Dacia Logan car. The study was made to choose the optimum excess air coefficient for the operation of gasoline injection engines. [5]

The calculation of the intake manifold pressure and the intake pressure in two cases was calculated; when the density of the motor fluid is constant and the case closer to reality when the density of the motor fluid is variable. In the program for calculating the parameters of the SI engine were the relationships in the second case. The three-dimensional variations of the pressure in the intake manifold p_{ga} and the inlet pressure p_a were represented according to the engine speed and the ambient temperature, at the value of the excess air coefficient $\lambda = 1$ and $p_o = 1 \cdot 102 \text{ kPa}$, resulting from the program in the annex B. With the program in Annex A, the three-dimensional variations of the pressure in the intake manifold p_{ga} and the inlet pressure p_a can be determined depending on the engine speed and the coefficient of excess air at ambient temperature to $= -35^\circ\text{C} \dots 45^\circ\text{C}$ and $p_o = 1 \cdot 102 \text{ kPa}$. Temperatures in the range -35°C and 45°C , are denoted by 5 in 5°C with $To1, To2 \dots To17$. [5]

The modelling the SI engine with gasoline injection proposed by the author consists in presenting the initial data of the calculate on program; calculating and correlating the

expressions of the parameters of the SI engine with the injection of gasoline for the implementation of the calculation programs in Annexes A and B. The calculation cycle of the proposed gasoline injection SI engine is an auxiliary cycle for the computer simulation of the gasoline injection. [5]

The computer simulation allows the determination of the proposed theoretical technical-economic parameters: the proposed theoretical mechanical work corresponding to the rounded diagram, the proposed theoretical pressure, the proposed theoretical efficiency, the proposed specific theoretical consumption. The pressures of mechanical and pumping losses are calculated, with the help of which the effective theoretical technical-economic parameters of the engine are calculated. [5]

By changing the conditions of the environment, the intake process is affected, there are changes in the combustion process, because the state conditions of the initial mixture change. As a result, the volumetric efficiency, the excess air factor, the indicated and efficient efficiency, ie all the factors that decide the level of power and specific fuel consumption will suffer deviations from their optimal values. In order to determine the optimal values for measurements, the atmospheric and altitude conditions under which these measurements are made and the net calorific value of the fuel must be taken into account.

Table 2. The comparison between the calculated and the real pressures in the characteristic points of the engine cycle.

The point	The calculated pressure [Pa]	The measured pressure [Pa]
<i>a</i>	81272	81200
<i>c</i>	1668684	1667000
<i>z</i>	5469207	5462000
<i>u</i>	3842592	3841000
<i>d</i>	363849	363000
<i>d_l</i>	114469	111300
<i>r</i>	114469	111400
<i>r_l</i>	81272	81200

It turns out that the differences between the two data sets are in the interval 0-2,68 %. The calculated value of the pressure at the end of the intake process is 0.09% higher than measured. The calculated pressure at the end of the compression stroke is 0.11% higher than measured. The pressure difference at this point is small, because in this part (until the end of the compression stroke) only small amounts of fuel burn and, therefore, no significant amount of heat is released.

The difference between the calculated and the measured value of the pressure at the end of the isochoric combustion, this is only 0.14%. However, the calculated value is higher than the measured value. At the end of post-combustion, the calculated pressure is 0.05% higher than the measured one.

These small differences explain the fact that in the engine during combustion there are other phenomena that could not be included in the calculation program, the amount of fuel burned in the isochoric phase is higher than the real one. In the post-combustion, in the theoretical cycle, a smaller amount of fuel remains to be burned. At the end of the expansion stroke, the calculated value of the pressure is higher than that measured by 0.24%.

The biggest difference is in the case of the exhaust pressure (2.68%). However, the calculated value is greater than the measured value. The values of the temperatures calculated in the characteristic points of the engine cycle were compared with those in the statistical data. It has been observed that the calculated values fall within the recommended ranges. For a better comparison between the calculated and the experimental data, the two diagrams were superimposed in Figure 16. [5]

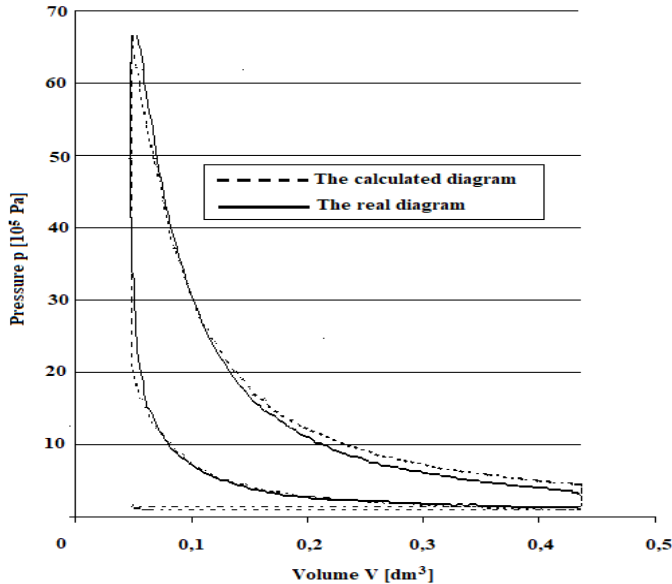


Figure 16. The overlap of the calculated and the measured indicated diagram.

Figure 16 shows that, at the end of the compression stroke, the difference between the calculated and the measured values is quite small (maximum 0.11%) and the area between the two curves is very small.

As mentioned earlier, this difference is due to the fact that the engine operating process is very complex and is influenced by many factors, which can influence the thermal processes in the engines.

A relatively large difference (maximum 2.5%) is also recorded at the beginning of the expansion race, corresponding to the delay in the theoretical cycle. This difference can be explained by the fact that the estimated amount of fuel burned in the actual cycle is higher than the theoretical one calculated are smaller than the real ones. There are some differences between the calculated and measured pressures in the second part of the expansion stroke, where the calculated values are higher than the measured ones (around 2.6%). The error can be reduced by changing the exponent of the expansion process.

The practical application of this calculus involves, on one hand, the improving of the physical-mathematical model, so that it will be as close as possible to the real development of the gasoline injection process. This means the reduction of the theoretical assumption and the calibration of some of the computation parameters, based on the experimental values. A theoretical model to compute with sufficient precision the thermal processes that take place in a SI engine can be useful for the development of new propulsion systems for road vehicles.

Many think that the transition to the full electric vehicles is a hybrid propulsion system. A variant is the inline hybrid propulsion system. In this case, the thermal engine should provide the energy to power the traction electric motor. The main advantage is the fact that the thermal engine can function at a single regime. This means that the adjustments that are necessary for the functioning at different regimes are no longer necessary. [10]

If it is possible the development of a model for the study of the ICE functioning at low or medium loads, it will be possible to determine the parameters that ensure minimum fuel consumption and polluting emissions at a specific functioning regime.

The model proposed in this paper, which proved to have a very good precision (and that can be improved) can be used to study the functioning of SI engines in different conditions.

The program was used for the study of other normally aspirated SI engines with gasoline injection.

The authors intend to use this model for turbocharged engines also.[10]

REFERENCES

- [1] Blaga V 2005 Engines with Gasoline Injection (Oradea: University of Oradea Publishing House)
- [2] Delanette M 1989 Les Motors a Injection (Edition Tehniques pour L'automobile et L'industrie)
- [3] Grunwald B 1980 The Theory, the Calculus and the Constuction of the Engines for Road Vehicles (Bucharerst: Didactic and Pedagogical Publishing House)
- [4] Mitran T, Blaga V and Moca S 2017 The Calculation Algorithm for the Determination of the Intake Stroke for GDI Engines (Brasov: International Congress of Automotive and Transport Engineering) pp 311-318
- [5] Blaga V 2000 Contributions to the Modelling of the Gasoline Injection at the SI Engines Cluj - Napoca: PhD Thesys)
- [6] Blaga V, Beles H, Dragomir G, Vlad I, Vlad M and Timar M 2009 The Theoretical Contribution Modelling Gasoline Injection at Spark Lightening (Viena: DAAM International Scientific Book) pp 43-58
- [7] Radcenko V 1977 Criteria for the Optimization of the Thermal Processes (Bucharest: Technical Publishing House)
- [8] Blaga V 2013 Processes and Characteristics of the Internal Combustion Engines (Oradea: University of Oradea Publishing House)
- [9] Blaga V, Bara L, Bara C, Bara V and Domuta C 2008 The Experimental Stand of Engines with Gasoline Injection (Viena: DAAM International Scientific Book) pp 109-110
- [10] Blaga V, Mitran T, Rus A, Beles H and Dragomir G. 2021 A comparative study of calculated and experimental indicated diagrams of a S.I. Engine AITS 2021 (Chisinau: IOP Conf. Series: Materials Science and Engineering); 1220 (2022) 012016.G



REVIEW OF THE ADVANCED HIGH-STRENGTH STEELS USED IN AUTOMOTIVE INDUSTRY

Djordje Ivković¹, Dragan Adamović², Dušan Arsić^{3*}, Nada Ratković⁴, Andjela Mitrović⁵, Ružica Nikolić⁶

Received in December 2023


Accepted in December 2023


RESEARCH ARTICLE


ABSTRACT: The objective of this paper was to present Advanced High-Strength Steels (AHSS) and their manufacturing processes, as well as to emphasize their complexity. The AHSSs were created as a solution to reduce the weight of parts and structures in transportation industries (automotive, airplane and truck industry). Regarding the development of the AHSSs, it was divided in three generation. Besides implementation of materials with higher strength, lower mass of structures could be achieved by application of materials of a lower density (e.g., aluminium and titanium). Application of the lightweight materials directly results in lowering the structures' mass, and it positively affects energy efficiency, preservation of the environment and lowering the pollution levels. However, there are still numerous problems and disadvantages, related to the application of lightweight materials, primarily with processing (low machinability, deformability, as well as weldability). Besides the processing problems, mentioned materials have higher prices than steel; therefore, development of new steel grades, as well as development of new methods for realizing the higher strength was initiated. It is already well known from the literature that by implementing the selected heat treatment procedures (varying the heating and cooling regimes), the steel properties could be altered. It was thus concluded that combination of the heat treatment and plastic deformation in steel production can result in increasing the steel strength, while simultaneously keeping the good deformability and even weldability.


KEY WORDS: AHSS, quenching, annealing, heat treatment, tempering

¹Djordje Ivković, University of Kragujevac, Faculty of Engineering, Sestre Janjić 6, 34000 Kragujevac, Serbia, djordje.ivkovic@fink.com,  <https://orcid.org/0000-0002-5747-7876>

²Dragan Adamović, University of Kragujevac, Faculty of Engineering, Sestre Janjić 6, 34000 Kragujevac, Serbia, adam@kc.ac.rs  <https://orcid.org/0000-0003-3459-3011>

³Dušan Arsić, University of Kragujevac, Faculty of Engineering, Sestre Janjić 6, 34000 Kragujevac, Serbia, dusan.arsic@fink.rs,  <https://orcid.org/0000-0003-0326-0898> (*Corresponding author)

⁴Nada Ratković, University of Kragujevac, Faculty of Engineering, Sestre Janjić 6, 34000 Kragujevac, Serbia, nratkovic@kg.ac.rs,  <https://orcid.org/0000-0003-1446-8678>

⁵Andjela Mitrović, University of Kragujevac, Faculty of Engineering, Sestre Janjić 6, 34000 Kragujevac, Serbia, andjamit99@gmail.com,  -

⁶Ružica Nikolic, University of Žilina, Research Centre, Univerzitna 8215/1, Žilina, Slovakia, ruzica.nikolic@uniza.sk,  <https://orcid.org/0000-0003-3042-8916>

PREGLED NAPREDNIH ČELIKA POVIŠENE JAČINE KORIŠĆENIH U AUTOMOBILSKOJ INDUSTRIJI

REZIME: Cilj ovog rada je da prikaže napredne čelike povišene jačine, načine njihovog dobijanja, kao i da ukaže na složenost pojedinih proizvodnih postupaka. Nastali su kao težnja da se smanji masa konstrukcija i delova koji se koriste u transportnoj industriji. Iz ugla razvoja, mogu se podeliti u tri grupe. Masa konstrukcija se osim upotrebom jačih materijala može smanjiti i primenom materijala koji imaju manju gustinu (npr. Al ili Ti). Upotreba lakih materijala direktno utiče na smanjenje mase i pozitivno deluje na povećanje energetske efikasnosti i prirodne sredine. Uprkos brojnim prednostima, postoje i nedostaci koji ograničavaju primenu ovih materijala. Ovi nedostaci su primarno vezani za proizvodne procese (smanjena obradivost rezanjem i deformisanjem, loša zavarljivost i sl.). Pomenuti laki metali, Al i Ti, osim pomenutih nedostataka imaju i visoku cenu u odnosu na čelike, te se njihovo polje primene dodatno sužava. Zbog svega gore navedenog započet je razvoj čelika povišene jačine kao i novih kombinacija mehanizama ojačanja koji dovode do porasta jačine čelika. Iz literature je poznato da se termičkom obradom može uticati na svojstva čelika, a u kombinaciji sa obradom deformisanjem na visokim temperaturama, uspevaju da se dobiju visoke vrednosti jačine i da se zadrži adekvatna plastičnost, a na nekim mestima čak i zavarljivost.

AHSS, quenching, annealing, heat treatment, tempering

KLJUČNE REČI: *AHSS, kaljenje, žarenje, termička obrada, otpuštanje*

© 2022 Published by University of Kragujevac, Faculty of Engineering

REVIEW OF ADVANCED HIGH-STRENGTH STEELS AND THEIR MANUFACTURING PROCEDURES

Djordje Ivković, Dragan Adamović, Dušan Arsić, Nada Ratković, Andjela Mitrović, Ružica Nikolić

INTRODUCTION

As the trends in modern industry are increasingly oriented towards the preservation of natural resources, increasing energy efficiency, reducing the harmful gases emission, as well as the carbon footprint, it is necessary to make adequate changes to fulfil the mentioned requirements. In the transportation industry, the change that effectively provides for these requirements to be met is related to reducing the mass of the steel structures. By using the composite or light-weight materials (Al, Ti and their alloys) that have the lower density and/or higher strength than steels, the mass of the structure can be significantly reduced. At the expense of the smaller mass, obtained by use of these materials, the production process is made more difficult due to their poor machinability by cutting and deforming, as well as poor weldability of the composite and light-weight materials, which all result in the price increase of the final product. To keep the processing method as simple as possible and the products' price as low as possible, development of the special high-strength steels started in the last decades of the 20th century. Compared to the classic steels, the new materials have significantly higher strength, with their machinability by cutting and deforming, as well as weldability, being at the required level [1]. The high strength of these steels is a result of the application of the complex thermal (heat), thermomechanical and mechanical processing procedures. Thus, the high strength allows the dimensions of the cross-sections of parts to be smaller; subsequently the amount of material used and the weight of structures became smaller. Regarding the industry of vehicle production, amount of AHSS used in vehicle body production increases each year (Figure 1). Nowadays, HSS are used in vehicles not only for body parts but for even more reliable components of the cars [2].

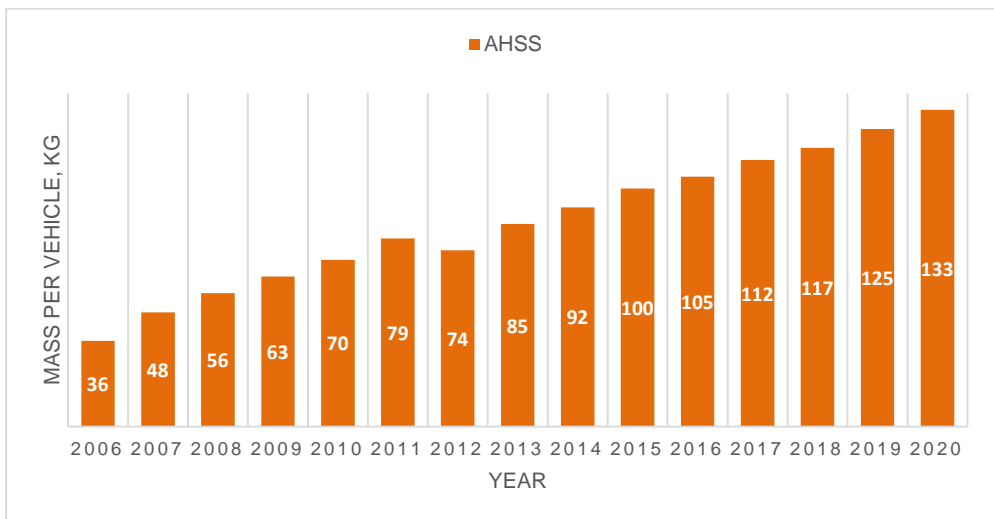


Figure 1. Amount of AHSS steel used in vehicle body production [1]

2. REVIEW OF THE GENERAL CHARACTERISTICS OF THE AHSS

2.1 The first generation AHSS

Sheets of tensile strength higher than 500 MPa belong to a group of the so-called high-strength steels (HSS). They possess a complex microstructure, which is usually composed of ferrite, bainite, martensite and residual austenite. The first generation AHSSs includes the Dual Phase steels (DP), Complex Phase steels (CP), Transformation Induced Plasticity steels (TRIP) and the martensitic steels. These steels were created as a result of the need for materials of a greater strength as compared to the classic steels. As with other steel materials, the rule applies here that as the strength increases, the plasticity decreases. From figure 2 one can conclude that the TRIP steels have the lowest strength but the highest plasticity, while for the martensitic steels the situation is quite opposite. They have the highest strength, but the lowest plasticity, [3].

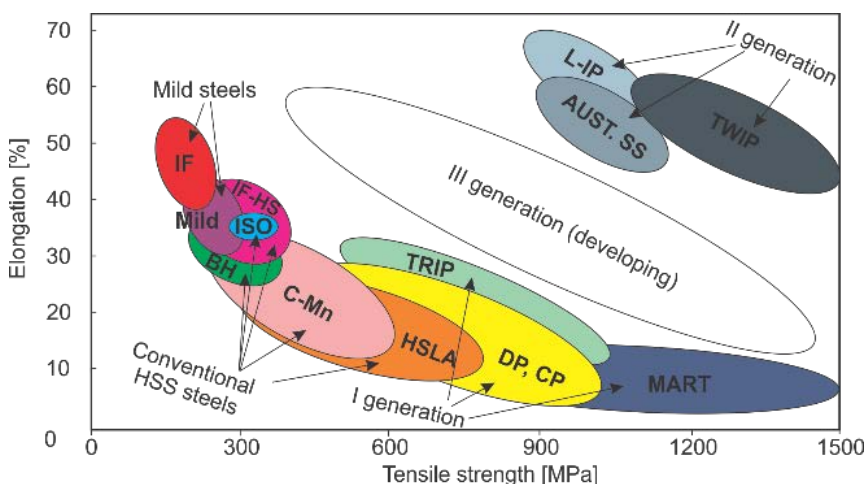


Figure 2. Mechanical characteristics of the advanced high strength steels [3]

2.1.1 The DP (Dual-phase) steels

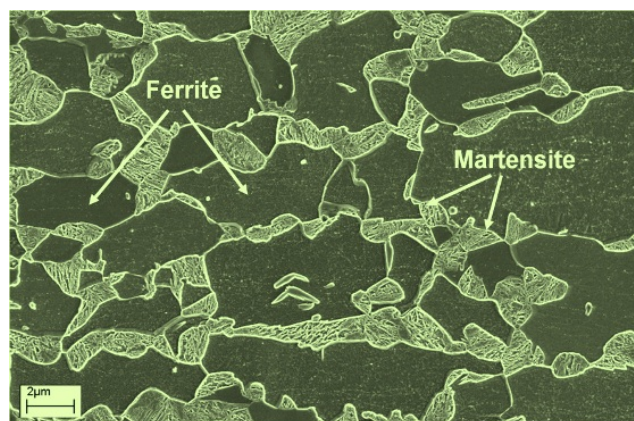
Due to the favorable relationship between the strength and plasticity, the DP steels have the greatest application in the automotive industry. The tensile strength value ranges from 420 to 1030 MPa, and the elongation from 5 to 28 %. The chemical composition of some of the DP steels is shown in table 1, while their mechanical properties are shown in table 2. The microstructure of the DP steel is made of a ferritic matrix containing martensite. The maximum share of martensite is 40 % and the steels' mechanical characteristics depend on it [3, 4]. An example of microstructure of the DP steel is shown in Figure 3.

Table 1. Chemical composition of certain DP steels' classes, wt% [4]

Designation according to EN 10336:2006	max C	max Si	max Mn	max P	max S	Al	max Cu	max B	max Ti+Nb	max Cr + Mo
HCT490X	0.14	0.5	1.8	0.05	0.01	0.01-1.5	0.2	0.005	0.15	1.0
HCT780X	0.18	0.8	2.5	0.05	0.01	0.015-1.0	0.2	0.005	0.15	1.4
HCT1180G2	0.23	1.0	2.9	0.05	0.01	0.015-1.0	0.2	0.005	0.15	1.0

Table 2. Mechanical characteristics of certain DP steels' classes [4]

Designation according to EN 10336:2006	$R_{p0.2}$, MPa	R_m , MPa	A_{80} , %
HCT490X	290-380	490-600	24
HCT780X	440-550	780-900	14
HCT1180G2	900-1100	1180-1350	5

**Figure 3.** Ferritic-martensitic microstructure of the DP steels [4]

2.1.2 The CP (Complex Phase) steels

These steels were so named due to their microstructure, which contains several different structural phases. The chemical composition of these steels is similar to composition of the DP steels. They are characterized by the high strength, while their plasticity is very low. They are the most widely used for production of columns and beams, as well as other simpler parts in the automotive industry [5].

The chemical composition as well as mechanical properties of some CP steels are shown in tables 3 and 4, respectively. As an example, the CP 800 steel microstructure is shown in Figure 4. It contains 42 % ferrite, 40 % bainite, 13 % martensite and 5 % residual austenite, [3, 5].

Table 3. Chemical composition of certain CP steels' classes, wt%, [5]

Designation according to EN 10346:2009	max C	max Si	max Mn	max P	max S	Al	max Cu	max B	max Ti + Nb	max Cr+Mo
HCT600C	0.1	0.4	1,6	-	-	-	-	-	-	-
HCT780C	0.18	1.0	2.5	0.05	0.01	0.15-1.0	0.2	0.005	0.15	1.0
HCT980C	0.23	1.0	2.7	0.05	0.01	0.015-1.0	0.2	0.005	0.15	1.0

Table 4 Mechanical characteristics of certain CP steels' classes, [5]

Designation according to EN 10336:2006	$R_{p0.2}$, MPa	R_m , MPa	A_{80} , %
HCT600C	360-440	600-700	19
HCT780C	570-720	780-920	10
HCT980C	780-950	980-1140	6

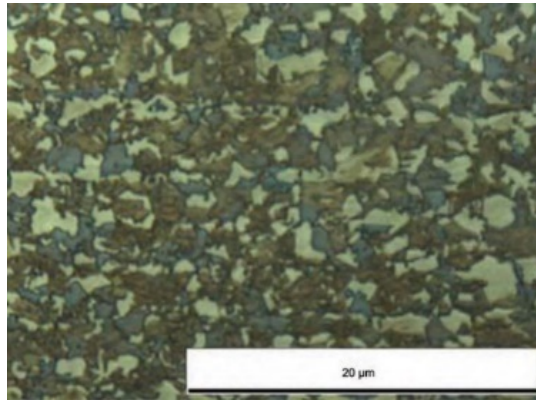


Figure 4. Microstructure of the CP800 steel [5]

2.1.3 The TRIP (Transformation Induced Plasticity) steels

Steels of this class contain carbon in the range of 0.1 to 0.4 % and alloying elements, such as Si, Al, Ti, Ni and V. Depending on the chemical composition of these steels, their strength ranges from 500 to 1050 MPa, and elongation from 12 to 32 %. Due to the good ratio of strength and plasticity, they are intended for the manufacturing the complex parts of automobile structures. The chemical composition and mechanical characteristics of some of the TRIP steels are presented in tables 5 and 6, respectively, [3,6].

The microstructure of the TRIP steels is complex. It basically consists of a ferrite-bainite matrix containing 5 to 20 % of the residual austenite. Thanks to this microstructure, these steels have good deformability properties. The share of ferrite in the ferrite-bainite matrix has the greatest impact on mechanical properties of these steels, [3, 6]. Figure 5 shows an example of the TRIP steel's microstructure.

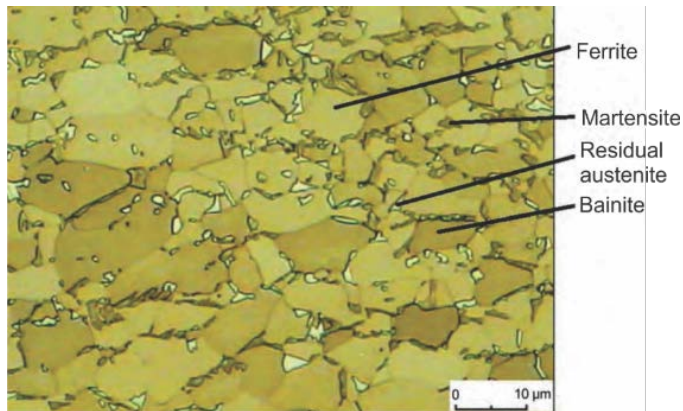


Figure 5. Example of TRIP steel microstructure [3]

A special feature of the TRIP steels is the increase in strength during deformation since the residual austenite is transformed into martensite [6]. That is why these steels are primarily used for production of the car body parts that are the most often exposed to deformation during a collision. The increase in strength of the parts during their deformation directly affects the increase in the safety of passengers in the car [3, 6].

Table 5. Chemical composition of the TRIP steels, wt%, [7, 8]

Designation according to EN 10346:2009	max C	max Si	max Mn	max P	max S	Al	max Cu	max B	max Ti + Nb	max Cr+ Mo
HCT690T	0.24	2.0	2.2	0.05	0.01	0.015-2.0	0.2	0.005	0.2	0.6
HCT780T	0.25	2.2	2.5	0.05	0.01	0.015-2.0	0.2	0.005	0.2	0.6

Table 6. Mechanical characteristics of the TRIP steels [7, 8]

Designation according to EN 10346:2009	$R_{p0.2}$, MPa	R_m , MPa	A_{80} , %
HCT690T	40-520	690-800	24
HCT780T	450-570	780-910	21

2.1.4 Martensitic steels

These steels were developed due to the need for steels with extremely high values of tensile strength. Their microstructure contains predominantly martensite, due to which the tensile strength of these steels is within range 720 to 1680 MPa, and the elongation is within range 3 to 15 %. The chemical composition and mechanical characteristics of some martensitic steels are shown in tables 7 and 8, respectively. Due to those exceptionally high mechanical properties, these steels are often subjected to tempering prior to forming, or the forming is done with preheating, and the forming itself is done in a tool that is cooled by the flowing water. In this way, the molded part obtains the martensitic structure, which comes as a result of the contact between the material in the initial state and the working surfaces of the tool [3, 9].

Table 7 Chemical composition of certain martensitic steels' classes, wt%, [9]

Designation according to VDA 239-100	max C	max Si	max Mn	max P	max S	Al	max Cu	max B	max Ti + Nb	max Cr+ Mo
CR1030Y130T-MS	0.28	1.0	2.0	0.02	0.025	≥ 0.010	0.2	0.01	0.15	1
CR1220Y1500T-MS	0.28	1	2	0.02	0.025	≥ 0.010	0.2	0.01	0.15	1
CR1350Y1700T-MS	0.35	1	3	0.02	0.025	≥ 0.010	0.2	0.01	0.15	1

Table 8 Mechanical characteristics of certain martensitic steels' classes [9]

Designation according to VDA 239-100	$R_{p0.2}$, MPa	R_m , MPa	A_{80} , %
CR1030Y130T-MS	1030-1330	1300-1550	3
CR1220Y1500T-MS	1220-1520	1500-1750	3

As emphasized at the beginning, these steels' microstructure is composed of a martensitic matrix containing small shares of ferrite and bainite. The martensitic steel CR1220Y1500T-MS microstructure is presented in figure 6.

2.2 The second generation AHSS

As it was shown, the first generation AHSS possesses great strength, but elongation and plasticity are low, especially for martensitic steels. Due to the lower plasticity, deformation rates during forming procedures such as bending and deep drawing are reduced and the risk of crack appearance is increased. In automotive industries, parts often have complex design and to produce such parts, greater plasticity is required, and researchers began developing the second generation AHSS.

Design of the second generation of AHSS is based on austenitic microstructure, which offers greater plasticity and formability in comparison to the first generation, but strength levels are not drastically reduced, [3]. The second generation of the AHSS includes the TWIP (TWinning Induced Plasticity) steels, L-IP (Lightweight Induced Plasticity) steels and austenitic stainless steels.

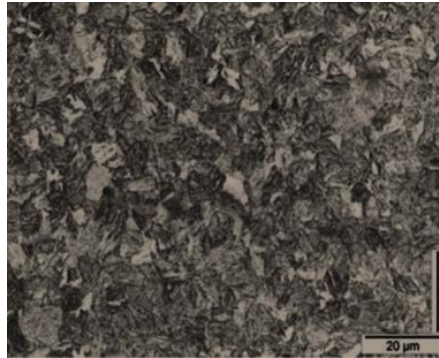


Figure 6. Microstructure example of the martensitic steels [3]

2.2.1 The TWIP (TWinning Induced Plasticity) steels

The TWIP steels have austenitic microstructure, which is retained at room temperatures due to high Mn content (22 % to 30 %). Besides Mn, the TWIP steels also contain fair amount of Al (maximum 10 %), as well as Si (maximum 3 %). Tendency to create twins in microstructure allows for the great strength to be achieved. Austenitic microstructure allows for elongation values to range from 60 to 90 % and their tensile strength exceeds 1000 MPa. The high strength results from austenitic microstructure ability to form twins, which are blocking movement of dislocation, thus increasing strength. [3, 10, 11].

The chemical composition and mechanical properties of some TWIP steels are shown in tables 9 and 10, respectively, and a microstructure example is given in figure 7.

Table 9. Chemical composition of some TWIP steels, wt%, [2, 9]

Designation according to BS	Mn	Si	Al	C
Fe -15Mn-4Si-2Al	16.2	4.0	1.8	0.2
Fe-20Mn-3Si-3Al	20.1	2.8	2.9	0.4
Fe-25-Mn-4Si-2Al	25.5	3.9	1.8	0.3
Fe-30Mn-4Si-2Al	28.7	4.0	2.0	0.2
Fe-30Mn-2Si-4Al	30.6	2.0	3.9	0.1

Table 10. Mechanical properties of some TRIP steels [2, 9]

Designation according to BS	$R_{p0.2}$, MPa	R_m , MPa	A, %
Fe -15Mn-4Si-2Al	190	1080	39
Fe-20Mn-3Si-3Al	300	840	82
Fe-25-Mn-4Si-2Al	280	770	69
Fe-30Mn-4Si-2Al	220	770	75
Fe-30Mn-2Si-4Al	210	570	83

2.2.2 The L-IP (Lightweight Induced Plasticity) steels

This steel group is still in development. Up to now, it is known that their strength ranges between 1000 to 1100 MPa, and elongation values reach up to 80 %. Application of this steel group could be found in automotive industry for producing parts with complex geometry, due to their good plasticity values [3].

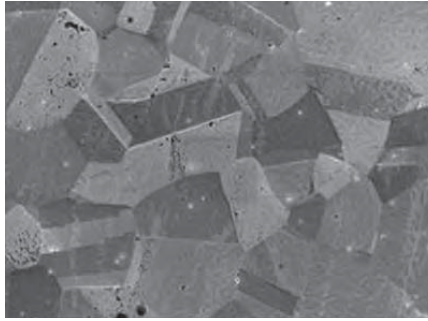


Figure 7. Microstructure of annealed Fe-30Mn steel [3]

2.2.3 Austenitic stainless steels

Austenitic stainless steels contain more than 12 % of Cr dissolved in solid solution, thus they are resistant to corrosion. This steel group besides Cr contains high values of Ni (max 35 %), which allows austenite to be stable at room temperatures. Addition of Ni drastically increases production costs due to its high price. Yield stress values range from 200 to 400 MPa, tensile strength values from 900 to 1200 MPa, and elongation values from 40 to 45 %. In comparison to other steels, they have good strength and formability with addition of corrosion resistance, so they can be used in more aggressive environment, [3]. The chemical composition and mechanical properties of some austenitic stainless steels are shown in tables 11 and 12, respectively, and microstructure example is given in figure 8.

Table 11. Chemical composition of some austenitic stainless steels, wt%, [12]

Designation according to EN 10088.2	max C	max N	max Mn	max Si	Cr	max Ni
X8CrNiS18-9	0.15	-	2.0	1.0	17-19	8-10
X5CrNi18-10	0.07	0.1	2.0	0.75	17.5-19.5	8-10.5
X8CrNi25-21	0.25	-	2.0	1.5	24-26	19.22
X5CrNiMo17-12-2	0.08	0.1	2.0	0.75	16-18	10-14

Table 12 Mechanical properties of some austenitic stainless steels [12]

Designation according to EN 10088.2	$R_{p0.2}$, MPa	R_m , MPa	A_{50} , %
X8CrNiS18-9	300	650	45
X5CrNi18-10	205	515	40
X8CrNi25-21	205	515	40
X5CrNiMo17-12-2	205	515	40

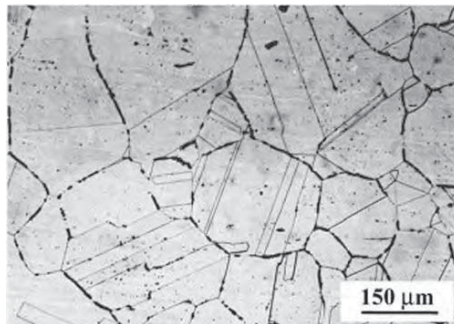


Figure 8. Microstructure example of austenite stainless steel [3]

2.3 The third generation AHSS

As the second generation AHSS is based on austenite microstructure, those steels contain high values of Cr and Ni to allow austenite to be stable at room temperature. The addition of mentioned components drastically increases price of steel, thus greatest disadvantage of second generation AHSS is their high price. Developing cheaper steels with similar properties represents the key for wider application of AHSS, [12].

Development of third generation AHSS is based on the goal to achieve similar plasticity of second generation AHSS, but with significantly lower price. The third generation AHSS includes Q&P (Quenching and Partitioning) steels, Medium Mn steels and Trip Aided Bainitic Ferrite (TBF) steels.

2.3.1 The Q&P (Quenching and Partitioning) steels

These steels typically contain C (0.1 - 0.3 %), Si and/or Al (1 - 2 %) as well as Mn (1.5 - 3 %). The yield stress values range from 600 to 1150 MPa, tensile strength from 980 to 1300 MPa and elongation from 8 - 22 %. One can conclude that strength values are higher than of the second-generation steels, with reduced formability. However, it needs to be emphasized that the price of the third-generation steels is significantly lower. Mechanical properties of some Q&P steels are given in table 13. Steels from this group are often used to produce parts of vehicle chassis such as B-pillars, [14].

Table 13 Mechanical properties of some Q&P steels [15]

Designation of steel	$R_{p0.2}$, MPa	R_m , MPa	A, %
QP980	698	1057	20
QP1180	990	1188	16

The microstructure of these steels is composed of austenite (5 - 12 %), ferrite (20 - 40 %) and martensite (50 - 80 %). As the ratio of mentioned phases changes, the steel's properties vary accordingly. Example of a microstructure is presented in figure 9.

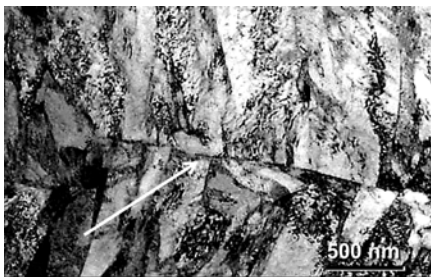


Figure 9. Microstructure of Q&P steel [16]

2.3.2 The medium Mn steels

This steel group has fine grain ferritic-austenitic microstructure. Percentage of austenite in microstructure can vary from 20 to 40 %, based on required properties and chemical composition. Typical for this steel group is that they contain C (0.05 - 0.4 %), Si (1- 3 %) and Mn (3 - 12 %). The yield stress values range from 400 to 1150 MPa, tensile strength from 780 to 1350 MPa and elongation ranges from 15 to 60 %. A microstructure example is given in figure 10, [14].

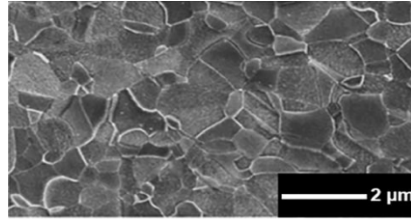


Figure 10. Microstructure of Medium Mn steel [17]

2.3.3 The TBF (Trip Aided Bainitic Ferrite) steels

The TBF steels are similar to Q&P steels and the first grades of this group were produced in Japan. The yield stress value is around 790 MPa, tensile strength around 1240 MPa, and elongation 16.5 %. These steels are alloyed with Mn, Al, Nb and Cr and their microstructure is composed of bainite, ferrite and austenite. The share of austenite has the great effect on plasticity and can be controlled through the carbon content. [18].

The chemical composition and mechanical properties of some TBF steels are given in tables 14 and 15, respectively. The microstructure of TBF steels is shown on figure 11.

Table 14. Chemical composition of some TBF steels, wt%, [19]

Designation according to VDA 239-100	max C	max Si	max Mn	max P	max S	Al	max Cu	max B	mac Ti + Nb	max Cr+ Mo
CR330Y590T-DH	0.15	0.8	2.5	0.05	0.01	0.015-1.0	0.2	0.005	0.15	1.4
CR440Y780T-DH	0.18	0.8	2.5	0.05	0.01	0.015-1.0	0.2	0.005	0.15	1.4
CR700Y980T-DH	0.23	1.8	2.9	0.05	0.01	0.015-1.0	0.2	0.005	0.15	1.4

Table 15. Mechanical properties of some TBF steels, [20]

Designation according to VDA 239-100	$R_{p0.2}$, MPa	R_m , MPa	A_{80} , %
CR330Y590T-DH	330-440	590-700	26
CR440Y780T-DH	440-550	780-900	18
CR700Y980T-DH	700-850	980-1130	13

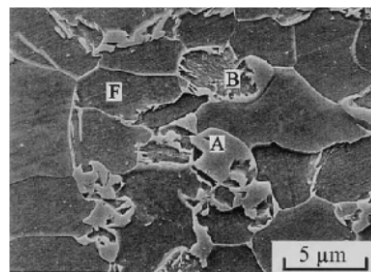


Figure 11. Microstructure example of TBF steel [3]

3. REVIEW OF PROCEDURES FOR OBTAINING THE THIN SHEETS OF INCREASED STRENGTH STEELS

3.1 Thermal and thermomechanical processes for obtaining the first generation AHSS

3.1.1 DP steels

The name of these steels indicates that there are two phases in their microstructure. That structure consists of a ferrite matrix in which martensite particles are wedged. The

maximum share of martensite in the microstructure of these steels is 40 %, and with that share increase in the microstructure, the strength and hardness increase, as well, [3].

The production of the cold-rolled DP steels is primarily based on the heating and heating-through of the previously obtained cold-rolled steel strips of the appropriate chemical composition, to a temperature in the interval between A_{c1} and A_{c3} . In this temperature interval, the microstructure of the steel consists of ferrite and austenite. With an increase in the heating temperature (approaching the critical temperature A_{c3}), the proportion of austenite increases, as well as the amount of carbon that can be dissolved in the austenite. To limit the share of martensite to 40 %, the maximum heating and heating-through temperature of these steels should be 800 °C, [3].

The heating-through is followed by cooling, where the cooling rate is higher than the critical one. In that way, the austenite with dissolved carbon forms martensite particles, which are distributed in the ferrite matrix. Figure 12 shows the thermal cycle for obtaining the cold-rolled DP steel, [3]. This first assumes that the appropriate semi-finished product from the ironworks is heated to a temperature between 1180 and 1250 °C, when it is rolled. After obtaining a strip of appropriate thickness, it is slowly cooled to a temperature between A_{c1} and A_{c3} , to obtain a mixture of ferrite and austenite in the microstructure. This is followed by the rapid cooling from that range, which results in the two-phase microstructure. The schematics of this procedure is presented in Figure 13, [2].

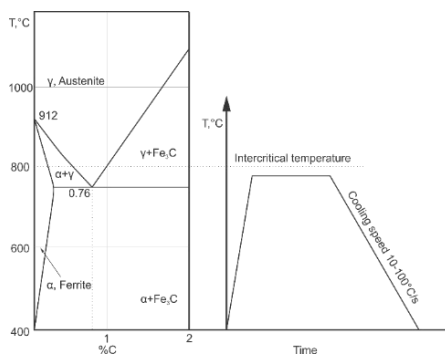


Figure 12. Thermal cycle for obtaining the cold-rolled DP steels [1]

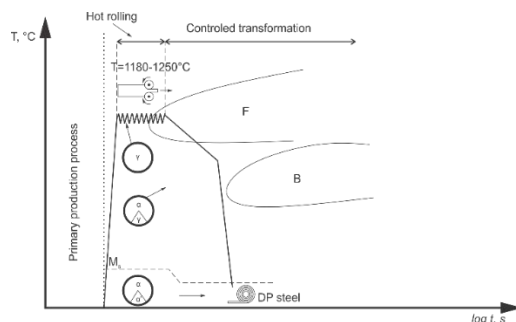


Figure 13. Schematics of producing the hot-rolled DP steels [2]

3.1.2 CP steels

The CP steels have an interphase microstructure. It consists of a ferrite-bainite matrix in which there are small shares of martensite, residual austenite and pearlite. Obtaining these steels implies that the starting semi-finished product is first heated to the high-austenitic temperature region, where the carbon content is 0.2 %. After the heating, the steel is cooled

down to a temperature between 900 and 800 °C, when it is rolled. After the rolling, the part is heated-through for 60 s, during which the ferrite-austenitic structure is obtained, and the carbon content increases to 0.4 %. The heating-through is then followed by the slow cooling to a temperature of 450 °C, where the steel is isothermally held for 90 s, which results in formation of a small share of bainite, and the carbon share increases to 1.2 %. After the isothermal holding, the thin strips are wound and then cooled to a room temperature. The thermal process of obtaining these steels is shown in Figure 14, [3].

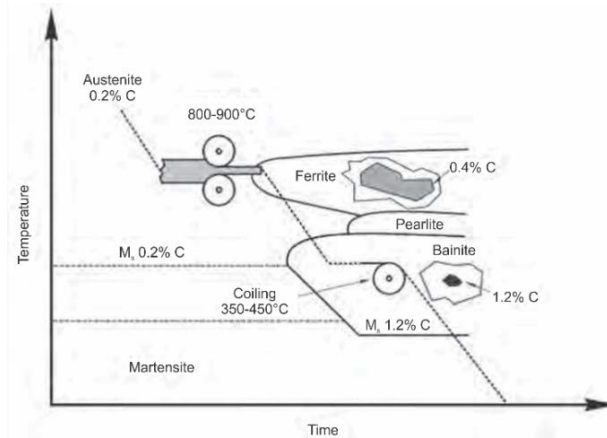


Figure 14. Thermomechanical process of obtaining the CP steels [3]

3.1.3 TRIP steels

The microstructure of these steels is also the interphase one. It is formed from a ferrite matrix in which the residual austenite and bainite are wedged. The process starts with rolling in the austenitic region, followed by cooling to 800 °C. At this temperature, the steel is heated-through for 60 s, which is followed by rapid cooling to 450 °C, where the steel is held isothermally for 90 s. This isothermal holding results in formation of a certain amount of bainite in the ferrite matrix. After the holding at 450 °C, the steel is wound to a coil and cooled to ambient temperature. The comparison of procedures for obtaining the DP and TRIP steel is schematically shown in Figure 15, [3].

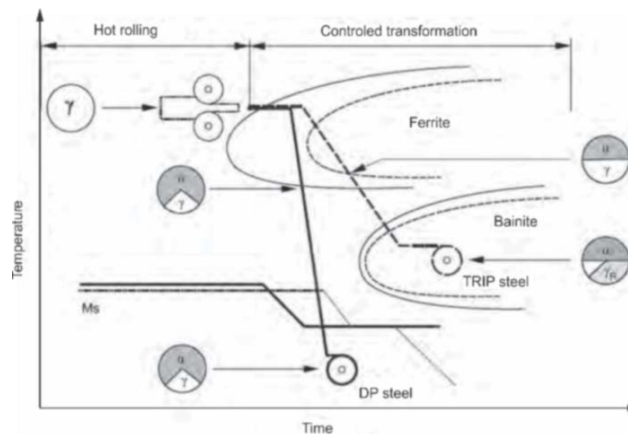


Figure 15. Comparison of production procedures of the DP and TRIP steels [2]

3.1.4 Martensitic steels

Steels of this kind predominantly contain martensite in microstructure. It is obtained in two ways, while both ways imply the rapid cooling of the steel from the austenite region.

The first way of obtaining such a microstructure refers to the hot-rolled steels, which are cooled down quickly, immediately after the rolling at elevated temperatures is finished, [3].

The second method implies that the previously obtained sheet metal strips are heated above the critical temperatures; they are then heated through at those temperatures and then cooled quickly, [3].

In both cases, due to heating to temperatures within the range 900 to 950 °C and rapid cooling, the final microstructure of the steel is martensite, [3]. Figure 16 shows the thermomechanical and thermal processes for obtaining these steels.

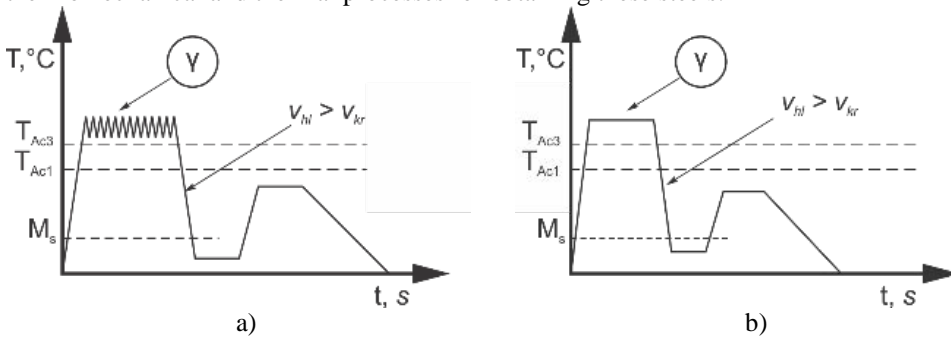


Figure 16. Thermomechanical (a) and thermal (b) procedures of obtaining the martensitic steels [3]

3.2 Thermal and thermomechanical processes for obtaining the second generation AHSS

3.2.1 TWIP steels

Typical procedure for obtaining the TWIP steels is based on appropriate thermomechanical procedure (Figure 17), which consist of the hot rolling, annealing, and quenching. the hot rolling is conducted in austenite region at 900 °C, afterwards follow the heating and annealing at 1150 °C. As annealing is finished, cooling in nitrogen gas is executed to obtain austenite. Water cooling could be conducted when martensite phase is required, [3].

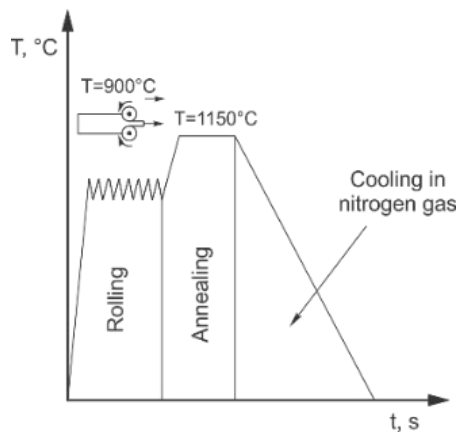


Figure 17. Example of thermomechanical procedure for TWIP steel production [2]

3.2.2 L-IP steels

For this steel group there is no much data available, as the fact is that they are still being developed.

3.2.3 Austenitic stainless steels

Steels of this group are obtained through already known procedures of continuous casting of liquid steel with proper chemical composition (Cr, Ni ...), with slight difference in the final production steps. For some austenitic stainless steels, the final step consists of the solution annealing at 1000 to 1100 °C to dissolve the formed carbides. The intense cooling is conducted from that temperature, without the phase transformation. [3]

3.3 Thermal and thermomechanical processes for obtaining the third generation AHSS

3.3.1 Q&P steels

The Q&P steels are obtained through the procedure, which consists of quenching and reheating. The quenching is done from austenite region to temperature between M_s and M_f , so that the slight amount of residual austenite is kept. After the quenching, steel is heated again to a temperature that is slightly above the M_s temperature, so that carbon, which is dissolved in residual austenite, could be partitioned into the acicular form [20, 21]. The typical heat treatment cycle is given in Figure 18.

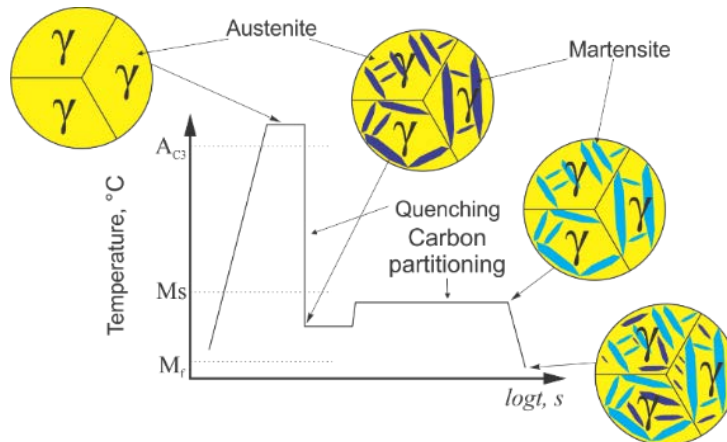


Figure 18. Thermomechanical procedure for production of Q&P steels [3]

3.3.2 Medium Mn steels

This steel group is produced through a special procedure (Figure 19), which begins with the hot rolling of the steel strip in austenite region. Through the initial hot rolling strips are rolled to thickness of 4 mm and temperature of the last pass needs to be higher than 800 °C. After the last pass, the strip is water cooled to room temperature. After the initial hot rolling, heating up to temperature interval from 700 to 800 °C is done and the strip is rolled down to required thickness. It needs to be emphasized that after each rolling, reheating to the mentioned temperature is required, to recover the deformed steel grains. After the final rolling, the steel strip is cooled down to room temperature and obtained steel microstructure consists of fine-grained ferrite-austenite microstructure, [22].

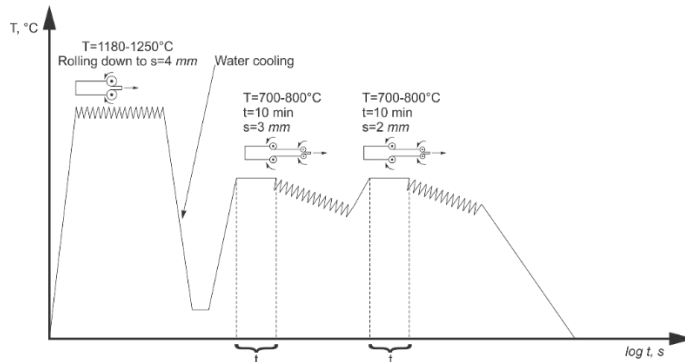


Figure 19. Example of thermomechanical procedure for producing Medium Mn steels [3]

3.3.3 TBF steels

The microstructure of these steels is based on a bainite matrix in which the residual austenite particles are dispersed. This structure is typically obtained through the fast cooling from austenite region to a temperature interval between B_s and B_f , and the isothermal holding on that temperature (Figure 20). The chemical composition and heat treatment parameters have the greatest influence on obtained microstructure phase shares, [23].

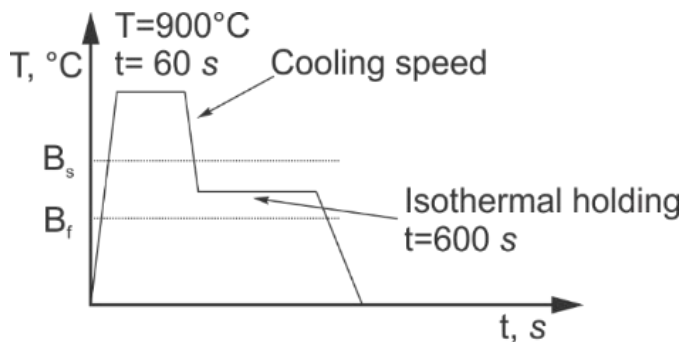


Figure 20. Example of thermal cycle for obtaining TBF steels [3]

4. CONCLUSIONS

Due to the increase in people's awareness of the necessity to reduce the environmental pollution, to use natural resources more rationally, development of the new steel materials, which compared to Al and Ti alloys, have a significantly higher specific mass and strength, but a lower price, better workability, and weldability (special requirements related only to cleaning and preheating of parts prior to welding), has been initiated. As an answer to this tendency, the new grades of advanced high strength steels (AHSS) have been developed. Depending on the level of development, three groups of advanced high-strength steels are distinguished. A review of all the three groups of AHSSs and some procedures for their production are presented. From the obtained data, one can conclude that all the three AHSS generations have high strength. However, deformability changes through generations.

The first generation of advanced high-strength steels has the greatest strength, but deformability is the worst among the three generations of mentioned steels.

The advanced high-strength steels of the second generation are characterized by slightly lower strength than the first-generation steels; however, they possess significantly better

deformability. Their greatest disadvantage is the very high price due to large amounts of alloying elements, especially Cr and Ni.

The third-generation steels represent the balance between the first two generations. Steels that belong to the third generation of advanced high-strength steel have good strength values (slightly below the first generation) and good deformability (slightly worse than the second generation). Their greatest advantage is the lower price as compared to the second generation, with the formability being good enough for producing the vehicle chassis parts.

Note: The shorter version of this research was presented at “The 39th International conference on production engineering of Serbia - ICPEs 2023”, reference [24].

ACKNOWLEDGEMENT

The authors wish to acknowledge the financial support from the Ministry of Education and Science of the Republic of Serbia through the project Grant TR32036 and TR35024 and by the project of Operational Programme Integrated Infrastructure “Support of research and development capacities to generate advanced software tools designed to increase the resilience of economic entities against excessive volatility of the energy commodity market”, ITMS2014+ code 313011BUK9, co-funded by European Regional Development Fund.

REFERENCES

- [1] Lesh, C., Kwiaton, N., Klose, F.: Advanced High Strength Steels (AHSS) for Automotive Application – Tailored properties by Smart Microstructural Adjustments; Steel Research International, vol. 88, no. 10, 1700210, 2017, doi:10.1002/srin.201700210.
- [2] Jovanović, S., Đorđević, Z., Kostić, S., Nikolić, D., Đorđević, M.: Selection of shaft materials using a multicriteria approach; Mobility & Vehicle Mechanics, vol. 48, no. 2, 33-40, 2022. <https://doi.org/10.24874/mvm.2022.48.02.04>
- [3] Demeri, M.: Advanced High-Strength Steels, Science, Technology and Application, ASM International, USA, 2013.
- [4] https://automotive.arcelormittal.com/products/flat/first_gen_AHSS/DP, Excerpts from the manufacturer’s catalogue ArcelorMittal, electronic form; accessed on 24.12.2021.
- [5] <https://www.ispatguru.com/dual-phase-steels/>, accessed on 24.12.2021.
- [6] https://automotive.arcelormittal.com/products/flat/first_gen_AHSS/CP, Excerpts from the manufacturer’s catalogue ArcelorMittal, electronic form; accessed on 24.12.2021.
- [7] https://automotive.arcelormittal.com/products/flat/first_gen_AHSS/TRIP, Excerpts from the manufacturer’s catalogue ArcelorMittal, electronic form; accessed on 24.12.2021.
- [8] D. Radović, Modern steels: Transformation induced plasticity, Welding and welded structures, 4/2011 pp. 167-170.
- [9] https://automotive.arcelormittal.com/products/flat/martensitic_steels/martinsite, Excerpts from the manufacturer’s catalogue ArcelorMittal, electronic form; accessed on 24.12.2021.
- [10] Radović, N., Glišić, D.: Modern steels - TWinning Induced Plasticity; Welding and welded structures, vol. 59, nr. 1, pp. 35-42, 2014. (in Serbian)

- [11] Grässel, O., Krüger, L., Frommeyer, G., & Meyer, L. W.: High strength Fe–Mn–(Al, Si) TRIP/TWIP steels development—properties—application; *International Journal of Plasticity*, vol. 16, no. 10-11, 1391-1409, 2000.
- [12] Atlas Steel, *Stainless Steel Grade Datasheets*, Atlas Steel Technical Department, August 2013.
- [13] Liu, B., Dai, Y., Huang, X., & Wang, Y.: Development of the third generation advanced high strength steel for automobile; 7th International Conference on Energy, Environment and Sustainable Development (ICEESD 2018), Shenzhen, China, March 30-31, 2018, vol. 163, pp. 1199-1202, Atlantis Press.
- [14] Bleck, W., Brühl, F., Ma, Y., & Sasse, C.: Materials and processes for the third-generation advanced high-strength steels; *BHM Berg-und Hüttenmännische Monatshefte*, vol. 164, no. 11, 466-474, 2019. <https://doi.org/10.1007/s00501-019-00904-y>. Springer.
- [15] Madrid, M., Van Tyne, C. J., Sriram, S., Pavlina, E. J., Hu, J., Clarke, K. D.: Hole expansion ratio in intercritically annealed QP 980/1180 steel grades as a function of testing condition; *IOP Conference Series: Materials Science and Engineering*, vol. 418, no. 1, p. 012083, 2018. doi:10.1088/1757-899X/418/1/012083
- [16] Bublíková, D., Jeníček, Š., Vorel, I., Mašek, B.: New heat treatment process for advanced high-strength steels; *IOP Conference Series: Materials Science and Engineering*, vol. 179, no. 1, p. 012009, 2017. doi:10.1088/1757-899X/179/1/012009
- [17] Tisza, M.: Three generations of advanced high strength steels in the automotive industry; *Vehicle and Automotive Engineering 3*, Proceedings of the 3rd VAE2020, Miskolc, Hungary, pp. 81-94, 2020. doi:10.1007/978-981-15-9529-5_7, Springer.
- [18] <https://ahssinsights.org/tag/tbf/>, accessed on 21.12.2021.
- [19] https://automotive.arcelormittal.com/products/flat/third_gen_AHSS/DH, accessed on 26.12.2021
- [20] Wang, L., Speer, J. G.: Quenching and partitioning steel heat treatment; *Metallography, Microstructure, and Analysis*, vol. 2, no. 4, 268-281, 2013.
- [21] Sun, J., Yu, H. Microstructure development and mechanical properties of quenching and partitioning (Q&P) steel and an incorporation of hot-dipping galvanization during Q&P process; *Materials Science and Engineering: A*, vol. 586, 100-107, 2013. <https://doi.org/10.1016/j.msea.2013.08.021>, Elsevier.
- [22] Hu, B., Luo, H., Yang, F., Dong, H.: Recent progress in medium-Mn steels made with new designing strategies, a review; *Journal of Materials Science & Technology*, vol. 33, no. 12, 1457-1464, 2017. <https://doi.org/10.1016/j.jmst.2017.06.017>, Elsevier
- [23] Bachmaier, A., Hausmann, K., Krizan, D., Pichler, A.: Development of TBF steels with 980 MPa tensile strength for automotive applications: microstructure and mechanical properties. Proceedings of the International Symposium on New Developments in Advanced High Strength Sheet Steels, June 23 - 27, 2013, Vail, CO, USA, pp. 23-27.
- [24] Ivković, Dj., Adamović, D. Arsić, D, Ratković, N., Nikolić, R.: Review of the first generation of the advanced high-strength steels (AHSS) and their manufacturing procedures; Proceedings of 39th International conference on production engineering of Serbia - ICPES 2023, 26-27 October 2023, Novi Sad, Serbia, pp. 181-188.



SIMULATION OF PEDESTRIAN THROW DISTANCE IN THE SOFTWARE PACKAGE PC-CRASH - COMPARISON WITH EXPERIMENT AND THEORY

Slavica Mačužić Saveljić^{1}, Danijela Miloradović²*

Received in August 2022

Revised in September 2022


Accepted in October 2022

RESEARCH ARTICLE

ABSTRACT: The application of software simulations in traffic accidents reconstruction is becoming more and more pronounced. The PC Crash software package stands out as one of the most widely used tools for this purpose in Europe. One of the most important items in the analysis of vehicle-pedestrian collision is the speed of the car at the time of the collision and its impact on the pedestrian throw distance. In this paper, the influence of selected vehicle and pedestrian parameters on pedestrian throw distance was simulated using the PC crash software. The simulation results were compared with available experimental and analytical results from other sources in order to validate the PC Crash model of the vehicle-to-pedestrian accident.

KEY WORDS: *Accidents, pedestrian, PC Crash, vehicle*

© 2023 Published by University of Kragujevac, Faculty of Engineering

¹Slavica Mačužić Saveljić, University of Kragujevac, Faculty of Engineering, 6 Sestre Janjić Str., 34000 Kragujevac, Serbia, s.macuzic@kg.ac.rs,  <https://orcid.org/0000-0003-2635-2496>
(*Corresponding author)

²Danijela Miloradović, University of Kragujevac, Faculty of Engineering, 6 Sestre Janjić Str., 34000 Kragujevac, Serbia, neja@kg.ac.rs,  <https://orcid.org/0000-0003-1427-9789>

SIMULACIJA DUŽINE ODBAČAJA PEŠKA U PROGRAMSKOM PAKETU PC-CRASH - POREĐENJE EKSPERIMENTA I TEORIJE

REZIME: Primena softverskih simulacija u rekonstrukciji saobraćajnih nezgoda sve je izraženija. Programski paket PC Crash ističe se kao jedan od najčešće korišćenih alata za ovu svrhu u Evropi. Jedna od najvažnijih stavki u analizi sudara vozila i pešaka je brzina automobila u trenutku sudara i njen uticaj na rastojanje odbačaja pešaka. U ovom radu simuliran je uticaj odabranih parametara vozila i pešaka na rastojanje odbačaja pešaka pomoću programa *PC crash*. Rezultati simulacije su upoređeni sa dostupnim eksperimentalnim i analitičkim rezultatima iz drugih izvora kako bi se verifikovao PC Crash model sudara vozila-pešaka.

KLJUČNE REČI: *nezgoda, pešak, PC Crash, vozilo*

SIMULATION OF PEDESTRIAN THROW DISTANCE IN THE SOFTWARE PACKAGE PC-CRASH - COMPARISON WITH EXPERIMENT AND THEORY

Slavica Mačužić Saveljić, Danijela Miloradović

INTRODUCTION

Pedestrians are the most vulnerable group of road users, especially because of their bodily insecurity. The increased number of traffic accidents involving pedestrians is the result of the increase in vehicle speed. Pedestrians account for about 24% of all seriously injured people in traffic, and when it comes to minor injuries, pedestrians account for about 11% [1].

The collision of vehicles and pedestrians leaves traces on both the vehicle and the pedestrians in the form of structural damage and in the form of injuries to the body. In order to determine the circumstances under which the accident occurred, it is necessary to analyse the both participants (the vehicle and the pedestrian). Due to the difference in mass between vehicles and pedestrians, as a result of an accident, pedestrian injuries are always more significant.

The most common classification of collisions includes: frontal collision (complete or partial), lateral collision and trampling. The kinematics of vehicle and pedestrian collisions depend on many factors, such as:

- vehicle shape,
- vehicle collision speed,
- pedestrian height,
- pedestrian speed,
- direction of pedestrian movement,
- position of the pedestrian at the time of the contact with the vehicle.

The impact of the vehicle on the pedestrian implies any contact of the body of the pedestrian with the vehicle. The strength of the injury depends on the age of the pedestrian. Older pedestrians over the age of 65 suffer significantly more injuries compared to younger pedestrians [1]. According to statistics in [2], the number of dead pedestrians aged 65 and over accounted for a total of 51% of the total number. Figure 1 [3] shows the death risk for pedestrians of different age depending on the impact speed. Given that elderly persons are often treated as a special group in traffic, numerous studies have been conducted on the influence of the age limit on the risk of injuries [4, 5].

Contemporary literature studies the relationship between vehicles and pedestrians. In [6] a mannequin model is used to assess the effect of impact velocity and mean deceleration on pedestrian throw distance. In [4], the authors were engaged in research on the dependence of the death outcome of pedestrians and the speed of the vehicle at the time of the collision in a completely frontal collision. They came to the conclusion that, as the speed of the car increases, so does the death rate of pedestrians. For example, at a speed of 50 km/h, the risk of death of pedestrians is twice as high as at a speed of 40 km/h, and four times higher than at a speed of 30 km/h. In [7], the authors also investigated the influence of vehicle speed and the speed of pedestrian movement on the occurrence of traffic accidents. Research [8] dealt with geometric modelling of accidents using various software packages. To simulate the

throw of pedestrians at the time of the collision with the vehicle, they used the software program PC Crash.

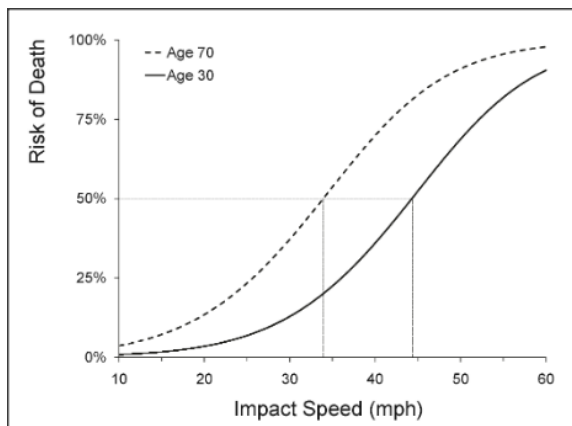


Figure 1. The percentage of pedestrian mortality depending on the impact speed [3].

In [9], an analysis of the distance of pedestrian throw based on the velocity speed was performed. Two databases were formed, one was a realistic measurement and the other database was formed based on simulations in the PC Crash software package. The results showed that there are differences in the use of these two bases by about 21%. However, the authors in [10] dealt with a similar analysis and came to the conclusion that there is a deviation of 10%. They concluded that the database used in the PC Crash software package could be used as a model for further data analysis.

In real conditions, in addition to the speed of the vehicle, it is necessary to include the braking distance, whether the vehicle has an ABS system or not and the pedestrian throw distance. Thus, in the paper [11], the authors reconstructed the vehicle-pedestrian collision using PC Crash and the exact value of the pedestrian throw distance was determined. They did a comparison of analysis data obtained in real conditions and with the help of simulation. The distance of pedestrian throw in real conditions was 11.2 m, while the simulation distance was 10.6 m. The deviation error was about 5%, which is allowed because, in the three-dimensional reconstruction of a traffic accident, when the error is less than 7%, the reconstruction is acceptable.

The paper [12] deals with the analysis of the variability of factors that influence the reconstruction of vehicle-pedestrian traffic accidents. Various anthropometric characteristics of the body were taken into account, such as height and weight, as well as the gender difference. Different positions of the pedestrian were analysed: - 0.5 m, 0 m, and + 0.5 m from the longitudinal axis of the vehicle, where 0 m corresponds to a central collision. Three different pedestrian movement speeds of 0, 2 km/h and 4 km/h were also taken into account, which correspond to a standing pedestrian, the pace of an elderly person, and a healthy person at a normal pace, respectively. Given that the coefficient of friction between pedestrians and road surface is always unknown, the following values were adopted: 0.4, 0.5, and 0.6. Based on the analysis, the results showed that four factors are significant for the experiment. These are: the height of the pedestrian, the angle of impact, the height of the vehicle hood, and the coefficient of friction between the pedestrian and the road surface.

Vehicle-pedestrian accidents account for more than 13% of the total number of accidents with victims [12]. In this paper, the PC Crash software was used as a vehicle-pedestrian

collision analysis software. PC Crash is software for traffic accident reconstruction analysis whose application has been recorded all over the world [13]. The technique of accident reconstruction is used in order to reduce the number of victims caused by these types of accidents. The latest technique, which is based on computer simulation, has reached a high level of development, the main goal of which is to determine the speed of a vehicle with a pedestrian collision [14]. In PC Crash, the pedestrian is modelled as a system of rigid bodies interconnected by joints [15, 16]. For the reasons mentioned, in this research, the distance of pedestrian throw was determined using the PC Crash software. The results obtained were compared to the results obtained by theory and by experimental research from [13] in order to verify the use of the mentioned software in vehicle-pedestrian accident reconstruction.

1. METHODS

The collision between a vehicle and a pedestrian is a complex event that is difficult to model. In order to develop effective measures to save pedestrians in traffic, it is necessary to properly understand the collision between vehicles and pedestrians. In addition, knowledge about the consequences of being exposed to a crash is required, as well as knowledge of the vehicle speed function itself. Knowledge of the mentioned measures provides useful information for the development of future pedestrian safety systems. It can also be used for designing vehicles and the pedestrian infrastructure itself.

In order to analyse the distance of pedestrian throw using the PC Crash, pedestrian modelling with body dimensions was performed, in the Multibody module. It is possible to get accurate information about the characteristics of the vehicle and the speed of the vehicle within the software database. Seven different vehicle speeds were taken into account: 38.46 km/h, 39.27 km/h, 43.61 km/h, 34.12 km/h, 55.04 km/h, 61.15 km/h and 64.86 km/h, while the weight of the pedestrian was 67 kg and the height was 1.78 m. The total weight of the vehicle was 1872 kg. Experimental data were taken from [13] for the purpose of comparison with simulation data.

The model of the Ford Crown Victoria 2005 vehicle was used in this paper. Figure 2 shows the loading of the vehicle into the PC Crash program, and figure 3 shows the setting of the vehicle speed.

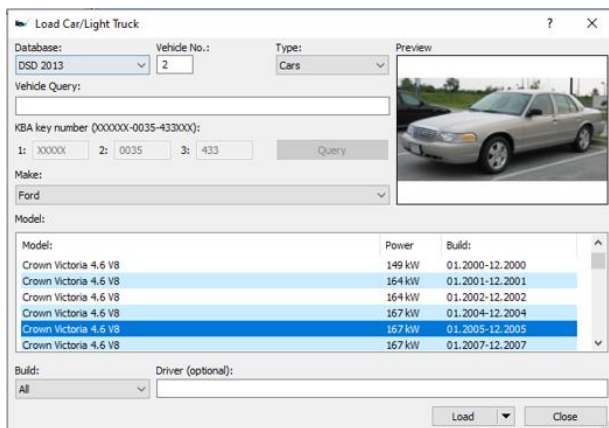


Figure 2. Importing the vehicle model into PC Crash software package.

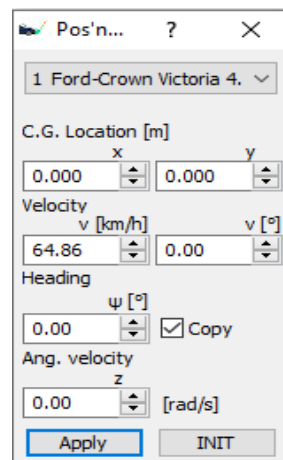


Figure 3. Setting the vehicle speed in the PC Crash software package.

In this paper, the frontal collision of vehicle and pedestrian was analysed. Based on various tests, the most commonly used theoretical dependence between the vehicle collision speed and the pedestrian throw distance can be presented in the following form [17]:

$$S_{od} = \frac{v_s^2}{144} (\pm 10\%), \quad (1)$$

where:

- S_{od} , m - distance from the place of collision to the final position of the pedestrian (pedestrian throw distance) and
- $v_s, \frac{m}{s}$ - impact speed.

Value 144 in equation (1) has the dimension of acceleration. Research has shown that equation (1) can be used for real accidents, but the results deviate by $\pm 10\%$.

In this paper, empiric Dekra formula (2) is used for the analytical calculation of the pedestrian throw distance [18] and various comparisons:

$$s = 2.5 + 0.38448 \cdot v + 0.05858 \cdot \frac{v^2}{a_{car}}, \quad (2)$$

where:

- $v, \frac{m}{s}$ - impact speed,
- s, m - pedestrian throw distance and
- $a_{car}, \frac{m}{s^2}$ - average car deceleration.

The three-dimensional Multibody model, which is a subroutine of PC Crash software, is based on the principle of biomechanics [19]. For this reason, it can be concluded that it is the best way to investigate this type of accident. Many input data are recommended as default data defined by the software, while others need to be entered by the user (figure 4).

After loading the pedestrian, it is possible to modify certain parameters of the pedestrian body. In the end, 3D-DXF models in PC Crash are used to make the simulation of a pedestrian-vehicle collision look as realistic as possible.

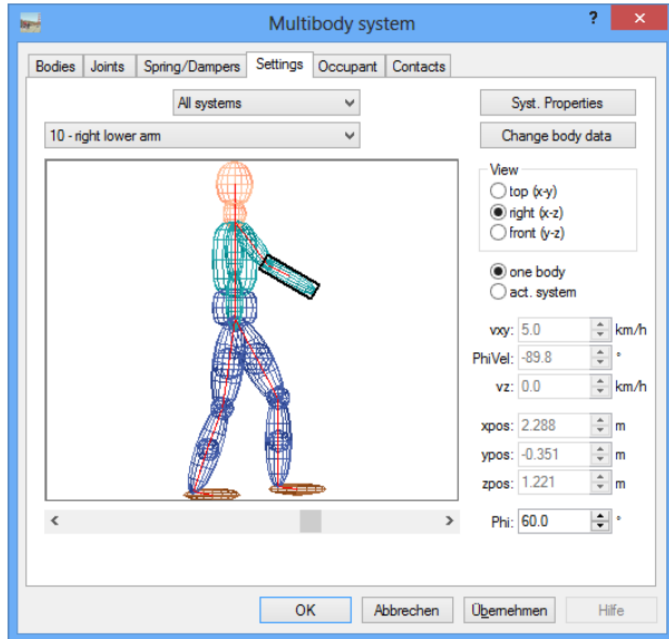


Figure 4. Input of pedestrian's parameters in the PC Crash software package.

2. RESULTS AND DISCUSSION

The obtained PC Crash software results for the pedestrian throw distance depending on the impact speed of the vehicle are shown in table 1, together with the data obtained experimentally [13] and analytically. After the analysis, a comparative presentation of all results was given.

Table 1. Values of pedestrian throw distance for different vehicle speeds

Test number	Vehicle impact speed, km/h	Pedestrian throw distance, m		
		Experimental [13]	Analytic	PC Crash
1	38.46	10.61	10.49	10.54
2	39.27	11.34	10.84	10.94
3	43.61	14.78	12.74	13.25
4	34.12	9.05	8.76	8.65
5	55.04	17.53	18.48	16.98
6	61.15	24.75	21.95	22.90
7	64.86	26.03	24.20	25.23

Based on table 1, it can be concluded that, as the impact speed of the vehicle increases, so does the throw distance of pedestrians. This increase was observed in all three types of analysis: experimental, analytical, and in the PC Crash program, figure 5.

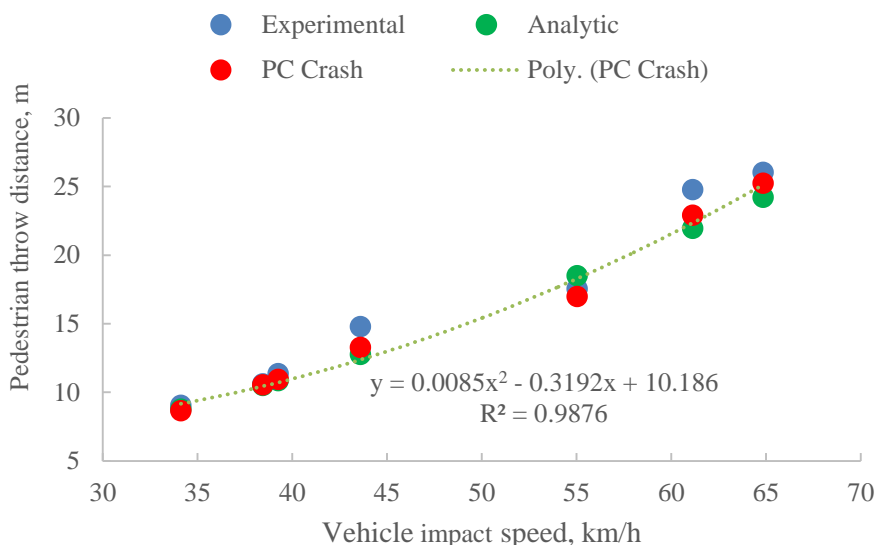


Figure 5. Pedestrian throw distance depending on impact speed.

Figure 5 shows a strong (parabolic) correlation between the pedestrian throw distance and the vehicle impact speed in PC Crash simulation results ($R^2=0.9876$). The smallest value of the pedestrian throw distance of 8.65 m was obtained numerically, using the PC Crash program, for impact speed of 34.12 km/h. The highest value of the pedestrian throw distance of 26.03 m was obtained by experimental determination, for impact speed of 64.86 km/h.

The descriptive statistical characteristics of pedestrian throw distance for the three observed types of results (standard error, sample variance, mean, standard deviation and kurtosis) are presented in table 2.

Table 2. Descriptive characteristics of pedestrian throw distance

	Pedestrian throw distance, m		
	Experimental	Analytic	PC Crash
Standard error	2.58	2.32	2.43
Sample variance	46.57	37.65	41.50
Mean	16.30	15.35	15.50
Standard deviation	6.82	6.13	6.44
Kurtosis	-1.42	-1.77	-1.27

Figure 6 shows relative deviations of the results for pedestrian throw distance obtained by analytical formula and PC Crash from the same results obtained by the experiment. It can be seen that the results of simulation done using PC Crash software show smaller deviations from the corresponding experimental data. Maximal relative deviation of the PC Crash simulation data is around 10%, while maximal relative deviation of the analytically obtained data is around 14%.

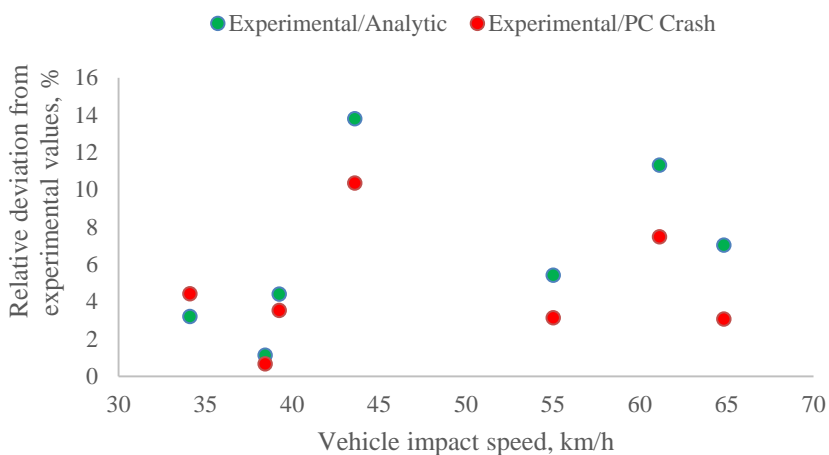


Figure 6. Relative deviation of the simulation data from the experimentally obtained values.

The analysis of the relative variations of the simulation results from the experimental data imply that the results obtained by using PC Crash software are closer to experimental data than data obtained by analytical calculations. This confirms the justification of using the PC Crash software in simulation of vehicle-pedestrian accidents when calculating pedestrian throw distances.

3. CONCLUSIONS

The application of computer programs for the analysis of traffic accidents enables a more precise analysis of the elements of the traffic accident, taking into account the place of the collision, the collision speed as well as the circumstances under which the traffic accident occurred.

PC Crash is a traffic accident simulation program that can simulate many traffic accident situations. In this research, PC Crash was used in the analysis of pedestrian throw distance depending on the impact speed of the vehicle. On the basis of simulations performed with different values of speed, pedestrian throw distances were obtained.

Based on various comparisons, it was found that the pedestrian model in PC Crash gives good estimates for determining the pedestrian throw distance, better than analytical model. Different vehicle shapes and pedestrian kinematics can be taken into account in the analysis. The pedestrian model in PC Crash proved to be easier to analyse, compared to the analytical way of analysis, because all the parameters that influenced the occurrence of the accident could be taken into account.

ACKNOWLEDGMENTS

This research was supported by the Ministry of Education, Science and Technological Development of the Republic of Serbia through Grant TR35041.

REFERENCES

- [1] Traffic Safety Agency of the Republic of Serbia 2021 *Overview Report - Pedestrian Safety in Traffic* (in Serbian)(Belgrade: Traffic Safety Agency of the Republic of Serbia) p 23
- [2] Traffic Safety Agency of the Republic of Serbia 2021 *Statistical Report on Traffic Safety in the Republic of Serbia in 2020* (in Serbian) (Belgrade: Traffic Safety Agency of the Republic of Serbia) p 117
- [3] Tefft B 2011 *Impact Speed and a Pedestrian's Risk of Severe Injury or Death* (Washington DC: AAA Foundation for Traffic Safety) p. 20
- [4] Rosen E and Sander U 2009 Pedestrian fatality risk as a function of car impact speed *Accident Anal. Prev.* **41** pp 536-42
- [5] Demetriades D, Murray J, Martin M, Velmahos G, Salim A, Alo K and Rhee P 2004 Pedestrians injured by automobiles: relationship of age to injury type and severity *J. Am. Coll. Surg.* **199**(3) pp 382–87
- [6] Otte, D 2004 Use of throw distances of pedestrians and bicyclists as part of a scientific accident reconstruction method, *SAE Technical Paper Series* 2004-01-1216
- [7] Elliott J R, Simms C K and Wood D P Pedestrian head translation, rotation and impact velocity: The influence of vehicle speed, pedestrian speed and pedestrian gait, *Accident Anal. Prev.* **45** pp 342– 53.
- [8] Živanović M, Trifunović A and Lazarević D 2014 Geometrical modelling of traffic situations using computers (in Serbian) *Proc. of International scientific conference Synthesis* 25-26 April Belgrade pp 918-21
- [9] Saulić N, Papić Z and Ovcin Z 2020 Pedestrian throw distance prediction from vehicle damage intensity *Promet – Traffic & Transportation* **32**(3) pp 371-82
- [10] Portal R J and Dias J M Pedestrian 2009 Reconstruction Tools Applied to Pedestrian Accidents in Portugal, *Proc. of the 3rd International Symposium on ESAR "Expert Symposium on Accident Research"* 5-6 September Hannover pp 304-14
- [11] Zhen L, Haibo H, Dan L and Pingfei L 2015 Analysis of Influencing Factors of Pedestrian-Vehicle Accident Reconstruction Based on Pc-Crash” *Proc. of International conference on education, management and computing technology ICEMCT* 13-14 June Tianjin pp 1576-80
- [12] Martínez F, Páez J, Furones A, Sánchez S Pedestrian-Vehicle Accidents Reconstruction with PC-Crash: Sensibility Analysis of Factors Variation *Proc. of XII Conference on Transport Engineering CIT 2016*, 7-9 June Valencia pp 115 – 21
- [13] Becker T, Reade M and Scurlock B 2015 Simulations of Pedestrian Impact Collisions with Virtual CRASH 3 and Comparisons with IPTM Staged Tests [arXiv:1512.00790v3](https://arxiv.org/abs/1512.00790v3) [physics.pop-ph]
- [14] Ziola A 2018 Verification of road accident simulation created with the use of PC-Crash software *Scientific Journal of Silesian University of Technology. Series Transport* **98** pp 211-21
- [15] DSD 2018 *PC-Crash – A Simulation program for Vehicle Accidents Operating Manual Version 12.0* (Linz: DSD, Dr. Steffan Datentechnik Ges.m.b.H.)
- [16] Happer A, Araszewski M, Toor A and Overgaard R 2000 Comprehensive Analysis Method for Vehicle/Pedestrian Collisions, *SAE Technical Paper Series* 2000-01-0846
- [17] Toor A and Araszewski M 2003 Theoretical vs. Empirical Solutions for Vehicle/Pedestrian Collisions *SAE Technical Paper Series* 2003-01-0883

- [18] Moser A, Hoschopf H, Steffan H and Kasanicky G 2000 Validation of the PC-Crash Pedestrian Model *SAE Technical Paper Series* 2000-01-0847
- [19] Wang X, Peng Y, Yu W, Xie P, Zhang H, Hu L and Quan Y 2020 The analyses of vehicle-to-pedestrian accidents by integrating rigid-body simulation and robust optimization techniques *Int. J. Comput. Methods* **17** 1950026

MVM – International Journal for Vehicle Mechanics, Engines and Transportation Systems
NOTIFICATION TO AUTHORS

The Journal MVM publishes original papers which have not been previously published in other journals. This is responsibility of the author. The authors agree that the copyright for their article is transferred to the publisher when the article is accepted for publication.

The language of the Journal is English.

Journal *Mobility & Vehicles Mechanics* is at the SSCI list.

All submitted manuscripts will be reviewed. Entire correspondence will be performed with the first-named author.

Authors will be notified of acceptance of their manuscripts, if their manuscripts are adopted.

INSTRUCTIONS TO AUTHORS AS REGARDS THE TECHNICAL ARRANGEMENTS OF MANUSCRIPTS:

Abstract is a separate Word document, “*First author family name_ABSTRACT.doc*”. Native authors should write the abstract in both languages (Serbian and English). The abstracts of foreign authors will be translated in Serbian.

This document should include the following: 1) author’s name, affiliation and title, the first named author’s address and e-mail – for correspondence, 2) working title of the paper, 3) abstract containing no more than 100 words, 4) abstract containing no more than 5 key words.

The manuscript is the separate file, „*First author family name_Paper.doc*“ which includes appendices and figures involved within the text. At the end of the paper, a reference list and eventual acknowledgements should be given. References to published literature should be quoted in the text brackets and grouped together at the end of the paper in numerical order.

Paper size: Max 16 pages of B5 format, excluding abstract

Text processor: Microsoft Word

Margins: left/right: mirror margin, inside: 2.5 cm, outside: 2 cm, top: 2.5 cm, bottom: 2 cm

Font: Times New Roman, 10 pt

Paper title: Uppercase, bold, 11 pt

Chapter title: Uppercase, bold, 10 pt

Subchapter title: Lowercase, bold, 10 pt

Table and chart width: max 125 mm

Figure and table title: Figure _ (Table _): Times New Roman, italic 10 pt

Manuscript submission: application should be sent to the following e-mail:

mvm@kg.ac.rs ; lukicj@kg.ac.rs

or posted to address of the Journal:

University of Kragujevac – Faculty of Engineering

International Journal M V M

Sestre Janjić 6, 34000 Kragujevac, Serbia

The Journal editorial board will send to the first-named author a copy of the Journal offprint.

OBAVEŠTENJE AUTORIMA

Časopis MVM objavljuje originalne radove koji nisu prethodno objavljivani u drugim časopisima, što je odgovornost autora. Za rad koji je prihvaćen za štampu, prava umnožavanja pripadaju izdavaču.

Časopis se izdaje na engleskom jeziku.

Časopis *Mobility & Vehicles Mechanics* se nalazi na SSCI listi.

Svi prispeli radovi se recenziraju. Sva komunikacija se obavlja sa prvim autorom.

UPUTSTVO AUTORIMA ZA TEHNIČKU PRIPREMU RADOVA

Rezime je poseban Word dokument, „*First author family name_ABSTRACT.doc*“. Za domaće autore je dvojezičan (srpski i engleski). Inostranim autorima rezime se prevodi na srpski jezik. Ovaj dokument treba da sadrži: 1) ime autora, zanimanje i zvanje, adresu prvog autora preko koje se obavlja sva potrebna korespondencija; 2) naslov rada; 3) kratak sažetak, do 100 reči, 4) do 5 ključnih reči.

Rad je poseban fajl, „*First author family name_Paper.doc*“ koji sadrži priloge i slike uključene u tekst. Na kraju rada nalazi se spisak literature i eventualno zahvalnost. Numeraciju korišćenih referenci treba navesti u srednjim zagradama i grupisati ih na kraju rada po rastućem redosledu.

Dužina rada: Najviše 16 stranica B5 formata, ne uključujući rezime

Tekst procesor: Microsoft Word

Margine: levo/desno: mirror margine; unurašnja: 2.5 cm; spoljna: 2 cm, gore: 2.5 cm, dole: 2 cm

Font: Times New Roman, 10 pt

Naslov rada: Velika slova, bold, 11 pt

Naslov poglavlja: Velika slova, bold, 10 pt

Naslov potpoglavlja: Mala slova, bold, 10 pt

Širina tabela, dijagrama: max 125 mm

Nazivi slika, tabela: Figure __ (Table __): Times New Roman, italic 10 pt

Dostavljanje rada elektronski na E-mail: mvm@kg.ac.rs ; lukicj@kg.ac.rs

ili poštom na adresu Časopisa
Redakcija časopisa M V M
Fakultet inženjerskih nauka
Sestre Janjić 6, 34000 Kragujevac, Srbija

Po objavljivanju rada, Redakcija časopisa šalje prvom autoru jedan primerak časopisa.

MVM Editorial Board
University of Kragujevac
Faculty of Engineering
Sestre Janjić 6, 34000 Kragujevac, Serbia
Tel.: +381/34/335990; Fax: + 381/34/333192
www.mvm.fink.rs